ISSN 0016-8521, Geotectonics, 2021, Vol. 55, No. 1, pp. 58–82. © Pleiades Publishing, Inc., 2021.
Russian Text © The Author(s), 2021, published in Geotektonika, 2021, No. 1, pp. 66–93.

Giant Quasi-Ring Mantle Structure in the African–Arabian Junction: Results Derived from the Geological–Geophysical Data Integration

L. V. Eppelbaum[a, *], Z. Ben-Avraham[a], Yu. I. Katz[b], S. Cloetingh[c], and M. K. Kaban[d, e]

[a] *School of Geosciences, Faculty of Exact Sciences, Tel Aviv University, Tel Aviv, Ramat Aviv, 6997801 Israel*

[b] *Steinhardt Museum of Natural History and National Research Center, Faculty of Life Sciences, Tel Aviv University, Tel Aviv, Ramat Aviv, 6997801 Israel*

[c] *Faculty of Geosciences, Utrecht University, 3584 CB Utrecht, The Netherlands*

[d] *Helmholtz-Centre Potsdam, GFZ German Research Centre for Geosciences, Telegrafenberg, Potsdam, 14473 Germany*

[e] *Schmidt Institute of Physics of the Earth, Russian Academy of Sciences, Moscow, 123242 Russia*

**e-mail: levap@tauex.tau.ac.il*

Received July 27, 2020; revised October 4, 2020; accepted October 29, 2020

Abstract—The tectonic–geodynamic characteristics of the North African–Arabian region are complicated by the interaction of numerous factors. To study this interaction, we primarily used satellite gravimetric data (retracked to the Earth's surface), which has been acknowledged as a powerful tool for tectonic–geodynamic zoning. The applied polynomial averaging of gravity data indicated the presence of a giant, deep quasi-ring structure in the Eastern Mediterranean, the center of which is located under the island of Cyprus. Simultaneously, the geometrical center of the revealed structure coincides with the Earth's critical latitude of 35°. A quantitative analysis of the obtained gravitational anomaly made it possible to estimate the depth of the upper edge of the anomalous body as 1650–1700 km. The GPS vector map coinciding with the gravitational trend indicates counterclockwise rotation of this structure. A review of paleomagnetic data on the projection of the discovered structure into the Earth's surface also confirms its counterclockwise rotation. Analysis of the geoid anomalies map and seismic tomography data commonly prove the presence of this deep anomaly. The structural and geodynamic characteristics of the region and paleobiogeographic data are consistent with the proposed physical–geological model. Comprehensive analysis of petrological, mineralogical, and tectonic data suggests a relationship between the discovered deep structure and near-surface processes. The deep structure also sheds light on specific anomalous effects in the upper layer of the crust, including the high-intensity Cyprus gravitational anomaly, counterclockwise rotation of the Mesozoic terrane belt, configuration of the Sinai Plate, and asymmetry of sedimentary basins along continental faults.

Keywords: satellite gravimetric data, geodynamics, tectonics, quasi-ring mantle structure, paleomagnetism, GPS, combined analysis

DOI: 10.1134/S0016852121010052

INTRODUCTION

Investigating the relationships between deep geodynamics and subsurface geological processes is one of the prime challenges in sciences of the solid earth [22, 23]. In this paper, we present a combined analysis of the North Africa–West Asia region, where giant tectonic plates (the Nubian, Arabian, and Eurasian), as well as a number of comparatively small tectonic units, interact [42]. This ~24 million km^2 region includes active faults and interacting tectonic belts, a complex pattern of continental and oceanic crust of different ages, intense seismic activity, and several high-amplitude gravitational anomalies; it is also characterized by significant seismic velocity deviations observed at great depths. In this region, zones of the final subduction phases and initial rifting (spreading) stages are comparatively close in location [13, 38, 43, 88, 91, 95, 106]. The geological–geophysical instability of this region, located in the junction zone between East Gondwana and Eurasia, is determined by geodynamic intensity—both collisional and rifting types (Fig. 1). Here, different fold belts and cratons have developed and diverse geological–geophysical processes are manifested [42, 59, 106, 108]. The Eastern Mediterranean is a tectonically complex region evolving in the midst of the progressive Afro-Eurasian collision, where the complex combination of different geological–geophysical elements requires application of integrated structural–geodynamic analysis by modern methodological and numerical methods.

Geophysical surveys of the Eastern Mediterranean have indicated an extensive zone of development of thinned continental crust [13] and identified a chain of the pre-Alpine terranes [13, 14]. At the center of the

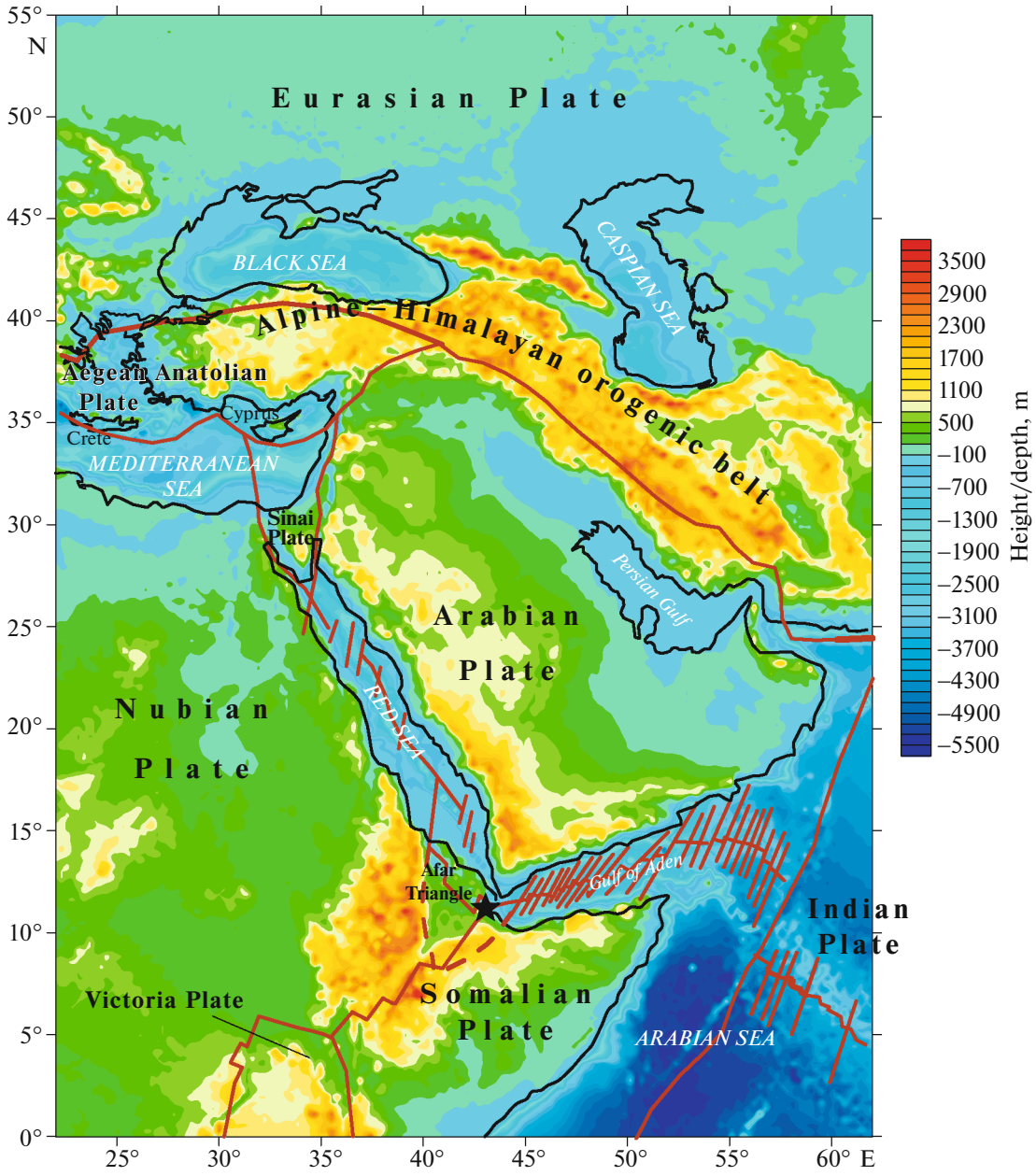

Fig. 1. Overview map of studied region with main tectonic elements.

Eastern Mediterranean is the high-intensity positive Cyprus gravitational anomaly (about 200 mGals in the Bouguer reduction) [46].

The aim of our article is an extended comprehensive analysis using geophysical methods (modeling of satellite and conventional gravity field anomalies, study of the distribution of geoid anomalies, analysis of the position of GPS vectors and paleomagnetic data, deformation of Earth's rotating ellipsoid, and deep geophysical mapping) and synthesis of various aspects of geological research (tectonic–structural zoning, tectonic–sedimentary reconstructions, geodynamic analysis, facies–paleobiogeographic mapping, utilization of geomorphological data, and involvement of a wide range of petrostructural, radiometric and mineralogical methods to study magmatic associations).

ANALYSIS OF SATELLITE GRAVITATIONAL ANOMALIES

Analysis of modern satellite gravimetric data is a powerful and effective tool for regional tectonic–geodynamic zoning, including data segmentation, transformation, and comprehensive tectonic–structural interpretation [18, 33, 34, 36–38, 60, 61].

The satellite gravimetric data for our study were obtained from the World Gravity DB as retracked from Geosat and ERS missions [97]. Examination of satellite data in a tectonic regional analysis in many cases makes it possible to detect essential peculiarities of the Earth's crust structure and thickness of the lithosphere [38, 61].

Eppelbaum and Katz [36] have shown that to study the deep structure in large regions (several million km^2 or more), satellite data retracked to the Earth's surface gravity can be used without any additional reductions. Initially, the studied Arabian–Northern African region was limited to the coordinates 0°–38° N and 30°–57° W [36, 38]. In both cited studies, various features of the Earth's crust and lithosphere were analyzed; however, they found no consistent relationships between the regional counterclockwise GPS pattern [27, 91] and the structure of the lithosphere. Therefore, it was concluded that the main source causing the GPS pattern may occur at large depths.

In this paper, we extended the study area to 0°–55° N and 22°–62° W. Analysis of the satellite gravimetric dataset involved several reliable mathematical tools, including polynomial approximation.

METHODS

Polynomial Approximation

Satellite gravimetric observations by a homogeneous network are the most suitable for mathematical modeling. The gravitational field of the studied region is caused by tens, perhaps hundreds of thousands of gravitational anomalies—is there some regional dominant anomaly among them? To better resolve the nature of these anomalies, we use the polynomial approximation, a powerful tool for solving a range of problems in mathematics and applied sciences [1, 7].

Polynomial computation identifies generalized trends in datasets. Processing of the aforementioned satellite gravimetric dataset (to construct the gravity map, more than 9.5×10^6 observations were compiled) practically eliminates numerous random components that can lead to errors in smaller datasets.

The anomalous gravity trend obtained with the polynomial cubic surface approximation (Fig. 2) is generally similar to results derived from distance weighting and nonlinear filtering. The main trend in all these processed gravity maps reflects a deep oval (quasi-ring) structure superficially reflecting a deep source of this anomaly. It should be noted that a comparable trend is reflected in a free air gravity map of long wavelength (800–3500 km) anomalies [76].

Quantitative Analysis of a Gravitational Anomaly

It is conventional practice, to interpret quantitatively transformed potential field anomalies [68, 111]. The depth of an anomalous source is associated with the width of the anomaly, inclination of its branches, square occupied by the area of the anomaly, and certain other parameters. The obtained gravitational anomaly was preliminarily analyzed using an improved tangent, characteristic point, and areal methods developed to examine potential geophysical anomalies in conditions where the level of the normal field is unknown [39]. Application of these methods indicated that the upper edge of the giant deep ring structure (GDRS) occurs at a depth of about 1650–1700 km, indicating that the anomalous source is in the lower mantle. Conventional quantitative interpretation methods [111] underestimated the depth of the upper edge by 10% (<1550 km). We call the projection of the GDRS onto upper geological sections (lithosphere and near-surface) as GDRSP.

Computations of Residual Gravitational Anomalies for the Lower Mantle

To verify the GDRS hypothesis, we computed the residual gravitational anomalies for the lower mantle. The gravitational effect of density variations in the lower mantle is hardly visible in the observed gravity field, since the latter one is dominated by heterogeneous density structure of the crust and upper mantle [60]. Another factor that also hides lower mantle effects is the dynamic topography induced by mantle flow [18, 60]. In particular, the effect of the dynamic topography is clearly visible in the residual isostatic anomalies computed for the Middle East and surrounding areas [60, 61]. Nevertheless, processing of large datasets makes it possible to refine patterns related to the lower mantle (Fig. 2). Another approach in this section makes it possible to remove crustal and upper mantle gravitational effects from the observed field and independently confirm the results obtained. This effect is computed by independent models obtained from various seismic data constrained by mineral physics [60].

The procedure of computing the residual gravity field consisted of two steps: (i) removal of the crustal gravitational effect (including topography/bathymetry) from the observed gravity field and (ii) computation of the residual gravitational anomalies for the lower mantle by removing the upper mantle effect from the total mantle field (the final map is shown in Fig. 3).

At the first stage, a 3D density model of the crust has been constructed for the Middle East and surroundings based on nearly all available seismic and geological data. This model was used to determine the gravitational effect of the crust with respect to a 1D reference density model, which was removed from the initial gravity field together with the effect of topography/bathymetry. Accordingly, the effect of the dynamic topography as part of the observed one is also excluded from the initial field [60].

Reduction of the gravitational effect of the upper mantle was based on available tomography models.

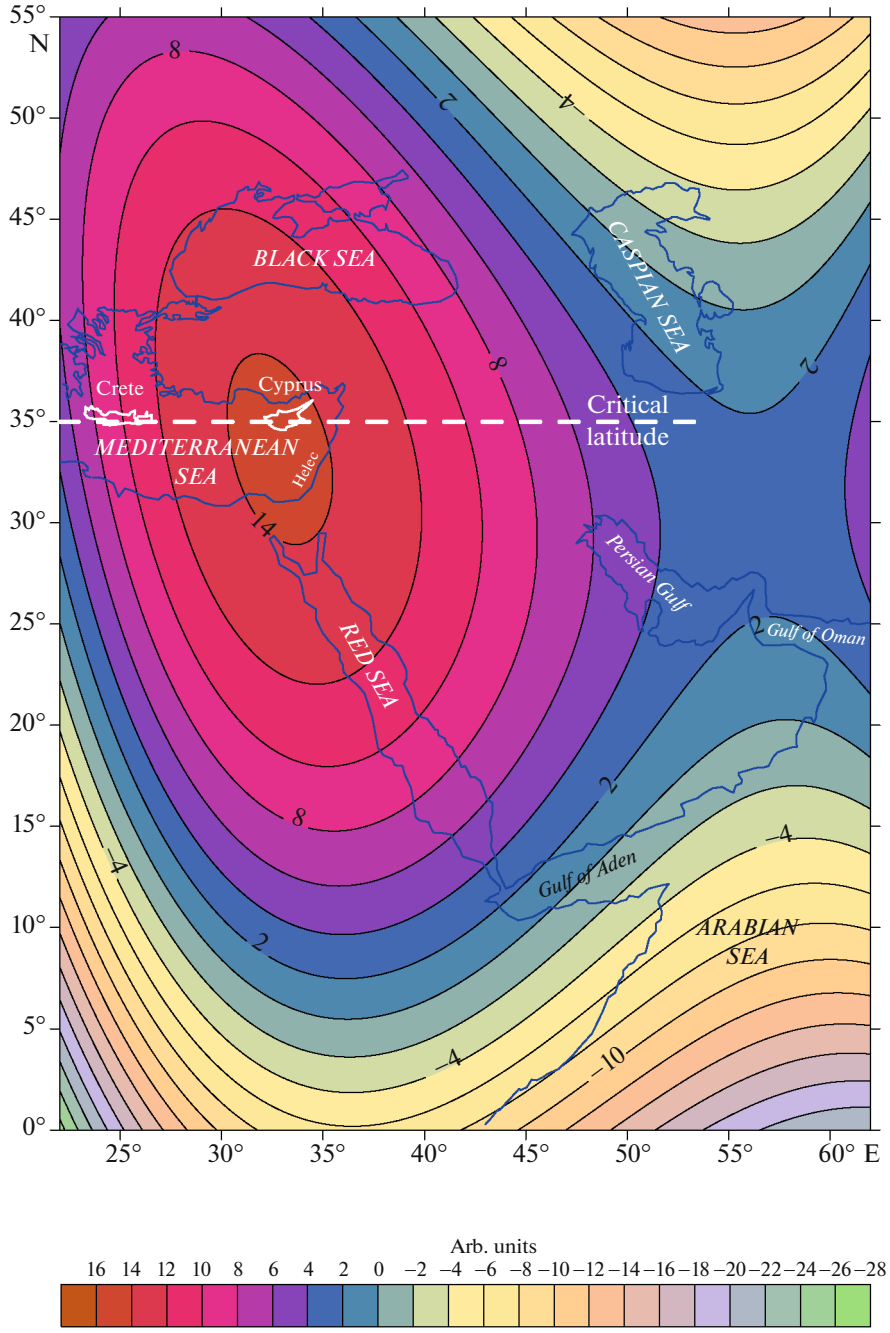

Fig. 2. Results of cubic polynomial approximation of satellite gravimetric data (white dotted line indicates position of critical latitude coinciding with the center of polynomial anomaly and the central region of Cyprus).

For this, we employed S-wave variations from the SL2013sv model [98]. For the depths less than 300 km, density variations were obtained by the mineral physics approach [112]. At great depths, where this approach does not work, a constant conversion factor obtained from the geodynamic modeling results was used to calculate the density:

$$\partial(\ln \Delta\rho)/\partial(\ln \Delta Vs) = 0.28, \quad (1)$$

where ρ is the density and *Vs* is the shear wave velocity [107].

The gravitational effect of the upper mantle with the transition zone (to a depth of 700 km) has been calculated with respect to the 1D reference model and removed from the total mantle anomalies [62] (the final results are shown in Fig. 3).

The most pronounced negative anomaly corresponds to the Gulf of Aden, while the northern part,

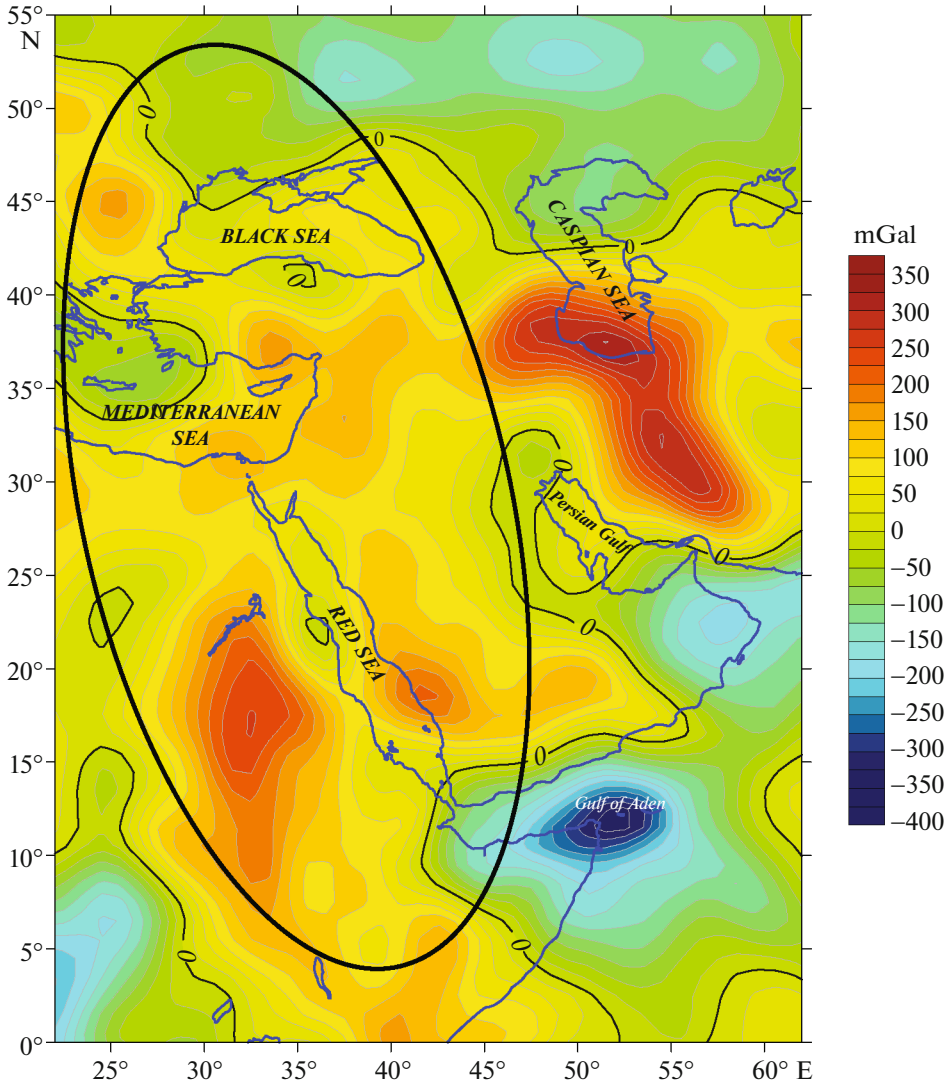

Fig. 3. Residual gravitational anomalies for lower mantle after removal of effect of the upper mantle (methodology is presented in [60]) from the total mantle field. The upper mantle gravitational anomalies were computed by the SL2013sv tomography model [98] as described in [61]. Black ellipse shows approximate location of the maximum in Fig. 2.

related to Eurasia and the Eurasia–Arabia transition zone, is predominantly characterized by significant positive anomalies (Fig. 3).

The lower mantle gravity field was significantly modified compared to the whole mantle anomalies. For example, the effect of the Afar plume is almost reduced, while South Eurasia after removal of the upper mantle effect is predominantly characterized by negative anomalies (Fig. 3). The residual gravity field is clearly divided into large and mid-scale anomalies, roughly dominated in the intervals >1000 and <400 km, respectively. The mid-scale anomalies cannot be generated by heterogeneity of the lower mantle due to the large distance to the original density anomalies. Obviously, they are related to the insufficient resolution of the initial tomography model and uncertainties in the velocity-to-density conversion [62]. Thus, we can select two groups of large-scale positive residual anomalies. The first group combines the maxima in the Eastern Mediterranean and in the vicinity of the Red Sea (Fig. 3). This broad anomaly agrees well with the residual anomaly revealed by the cubic polynomial approximation (Fig. 2) of the initial gravity field as shown by the black ellipse in Fig. 3. Therefore, this analysis also confirms the presence of the deep dense structure in the lower mantle in the study area. Another strong positive anomaly (right side of Fig. 3) is localized within the Arabia–Eurasia collision zone.

Analysis of the Geoid Anomaly Map

Generalized geoid anomalies (compiled on the basis of the EMG2008) and their comparison with the GPS data are shown in Fig. 4. It is well known that

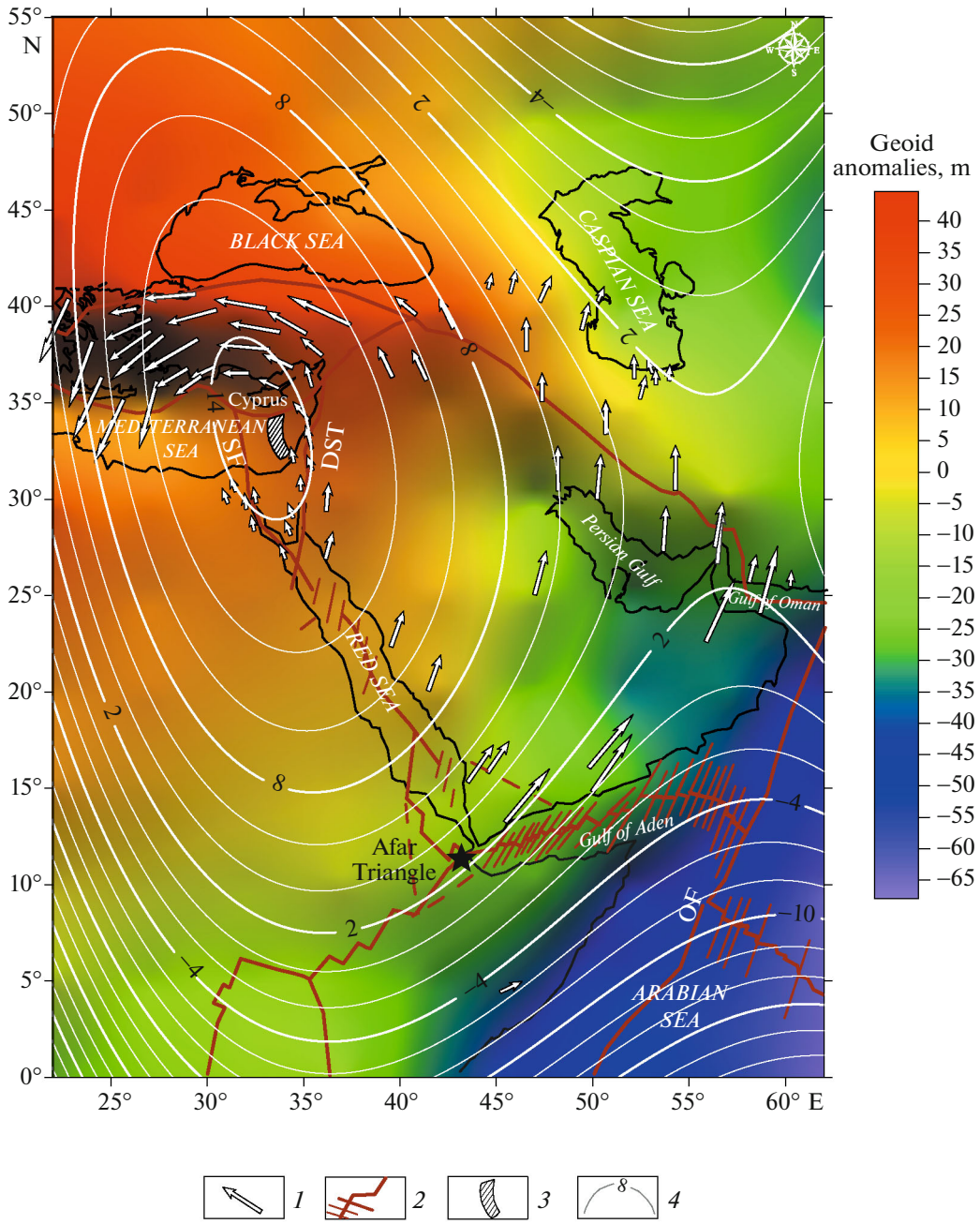

Fig. 4. Map of geoid anomalies (compiled from EMG2008 [126]) combined with the GPS pattern, isolines of gravity trend, and main tectonic elements. (*1*) GPS vector pattern [27, 91], (*2*) main intraplate faults, (*3*) Kiama paleomagnetic hyperzone of inverse polarity [34], (*4*) isolines of gravitational trend obtained by cubic polynomial approximation. SF, Sinai Fault; DST, Dead Sea Transform; OF, Owen Fault.

the geoid map reflects integrated effects from the Earth's crust, mantle, and core [93]. The behavior of the geoid isolines (Fig. 4) displays a large quasi-circular anomaly (see Fig. 4). In general, elevations of the geoid reflect the arch of the deep structure, and lows—the periclinal part.

Geodynamically, this map (Fig. 4) agrees nicely with the GPS data pattern, polynomial gravitational anomaly (shown by white isolines in Fig. 4) and residual gravitational anomalies calculated for the lower mantle (see Fig. 3). The geoid anomalies also correlate to a large extent with the regional tectonic elements presented in this figure.

The geoid isolines show an elongated zone from the NNE to SSW separating areas of positive and negative geoid values. These inhomogeneities in the deep mantle have been previously interpreted as the planetary Ural–African Step [64]. At present, based on analysis of GPS, paleomagnetic, and seismic data (see below), we suggest that such a behavior of geoid iso-

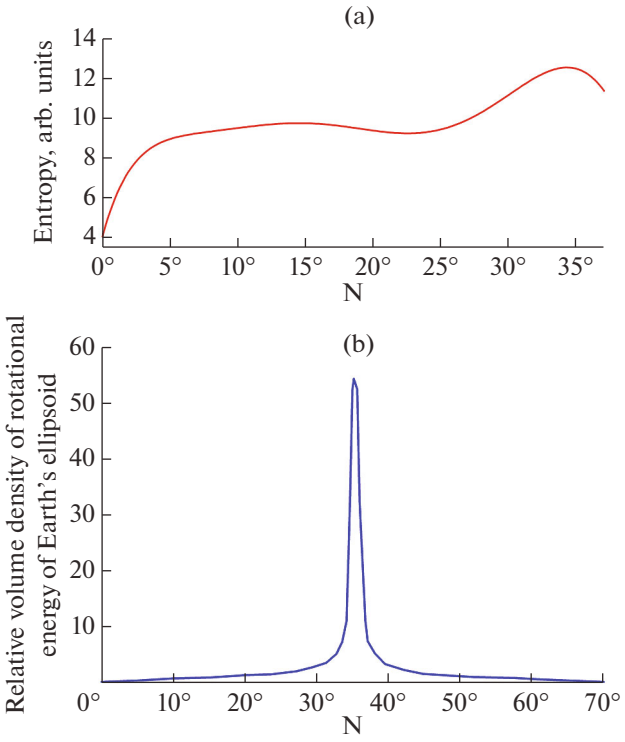

Fig. 5. Graphs of dependence of entropy and relative volumetric density of rotation energy of the Earth's ellipsoid on latitude. (a) Empirical graph of the entropy changes vs. latitude calculated from satellite gravimetric data for the Eastern Mediterranean (according to [38]); (b) Dependence of the relative volumetric density of the rotation energy of the Earth's ellipsoid on latitude (according to [77]).

lines is caused by the integrated effect of the Ural–African Step (minor) and deep ring structure (major), the upper edge of which occurs at a depth of about 1700 km.

CRITICAL LATITUDE OF THE EARTH

Véronnet [120] carried out a detailed physicomathematical analysis of the Earth's ellipsoid of revolution and showed that the most critical latitude is ≅35°. According to [120], this is due to changes in velocity of the Earth's rotation and uneven effect of the tidal forces. Further studies using extensive material (e.g., [4, 64, 67]) confirmed that, in accordance with Véronnet's theory, periodic matter fluxes in the Earth's mantle move out from the equatorial to the polar region and vice versa. Critical parallels ≅±35° form the most active geodynamic zones of conjugate deformation of the Earth's ellipsoid of revolution, unchanged in the cross-sectional area of the Earth.

On the basis of the calculated entropy map (as an information measure of uncertainty) using the well-known formula

$$H_i = -\log_2 p_i, \qquad (2)$$

where p_i is the relative probability of an event (a physical quantity) [68] and H is the satellite gravity field [38], an empirical graph of the dependence of the entropy value on latitude was plotted (Fig. 5a). Obviously, the Earth's critical latitude is not the only factor influencing the calculated entropy values, but in general the graph well illustrates the increase in entropy at the latitudes close to 35°.

Levin et al. [77] analyzed the features of critical latitudes (≅+35° and ≅–35°) in the Earth's ellipsoid of rotation and showed the relationship between the magnitudes of bulk compression and the angular velocity of rotation, as well as an increase in seismic activity at and near critical latitudes. They identified two critical zones in which the peak density of the energy of geoid rotation is recorded: for the Northern Hemisphere ≅+35° (see Fig. 5b), and for the Southern Hemisphere ≅–35° (in the latter zone, the distribution pattern of density values is symmetrical to the distribution shown in Fig. 5b). This value fully coincides with that of the critical latitude revealed earlier according to [120]. The center of the revealed deep structure practically coincides with the latitude of 35° (Fig. 2).

We consider it important to note that the center of the gravitational anomaly calculated for the lower mantle and corresponding to the middle of the Arabia–Eurasia collision zone also corresponds to the latitude of 35° (Fig. 3).

INTEGRATED ANALYSIS OF GEOPHYSICAL–GEOLOGICAL DATA

Geodynamic Analysis

Geodynamic analysis of global geological structures [2] indicates that arched segments are usually the most unstable zones (especially in the case of rotation). The Red Sea spreading zone is sharply outlined by an intense trend of the Bouguer anomalies [79] (Fig. 6c) and coincides with the long axis of the anomalous regional gravity trend derived from satellite gravitational anomalies (Fig. 6a), at the center of which is the high-amplitude Cyprus gravitational anomaly [47] (Fig. 6b). Thus, there was a good agreement between three types of independently observed gravimetric data.

The map in Fig. 6 is completely consistent with other geological–geophysical data, indicating asymmetry of the structure and movements of both sides of the neotectonic rifting zone in the Red Sea region (Fig. 6c). Within the axial zone of the rift (where there is no granite layer of the crust), the Bouguer anomalies reach almost +100 mGals [19] (Fig. 6c). With a sharp drop of the crust density due to intensified block movements and formation of the sliding and fractured elements of the breaking lithosphere, the magnitudes of the Bouguer gravitational anomalies shift sharply towards negative up to extremely negative values southwest of the Afar triple junction zone.

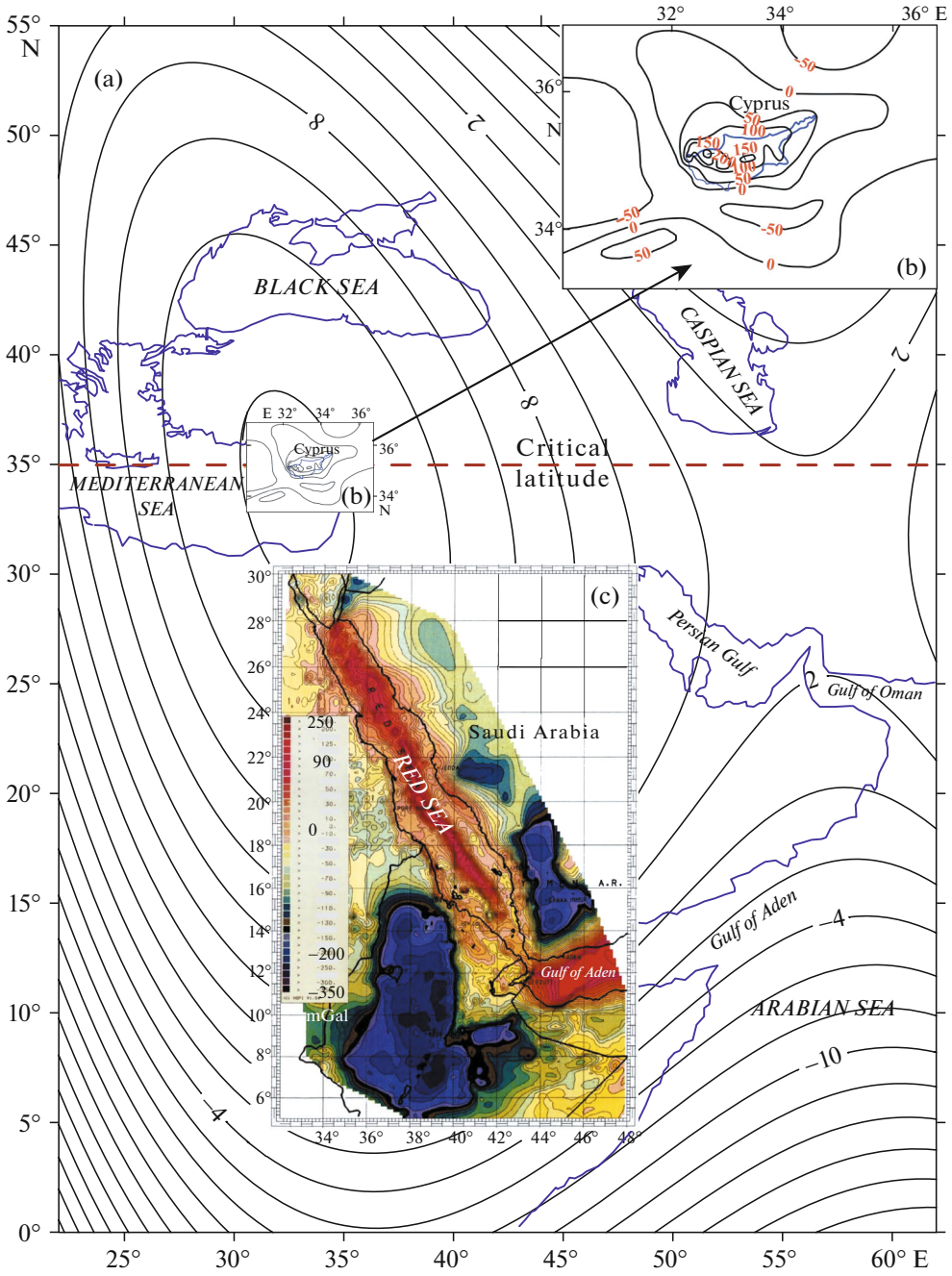

Fig. 6. Comparison of gravitational anomalies: (a) Polynomial trend derived from the satellite gravimetric data (see Fig. 2); (b) Cyprus isostatic gravitational anomaly (land/sea), after [47]; (c) Bouguer anomalies observed in the Red Sea and adjacent areas (sea/land) [79].

Analysis of the Bouguer anomalies in the western and eastern frames of the Red Sea crosscutting the system of igneous and metamorphic complexes of the Neoproterozoic belt (Fig. 7) clearly shows regional asymmetry in the distribution of the gravity field characteristics (see Figs. 6, 7). In the west, within the Nubian Plate, the Bouguer anomalies are close to stable platform values: ±50 mGals. In sharp contrast to these data, on the eastern coast, corresponding to the Arabian Plate (where extended fields of the Late Cenozoic dikes and effusive traps have developed), the Bouguer anomalies, which are linearly elongated parallel to the Red Sea coast, are characterized by pronounced negative values, which is typical for activated platforms.

The Red Sea spreading zone also contains signs of deep geodynamic activity: the earthquake epicenters at great depths (from 150 to more than 600 km) [30, 49,

119, 125] (Fig. 7). Despite the small amplitude of these earthquakes (M ≤ 3), this is an additional argument that the deep ring structure influences the overlying geological formations. Most of the deep-focus earthquakes are concentrated in the axial part of the deep structure, and earthquakes with the greatest depths (300–600 and >600 km) (except for two geodynamic events in the Persian Gulf region) completely coincide with this axial part of the deep structure (Fig. 7).

Figure 7 shows a combined tectonic–geodynamic–paleomagnetic sketch map of the region superimposed on the gravitational trend isolines. The elements of rotational dynamics obtained from analyzing the paleomagnetic data are mainly characterized by counterclockwise rotation and are consistent with the orientation of GPS vectors.

The plate tectonics reconstruction data [106] generally correspond to views on the modern regional geodynamics to the Arabian junction zone of Laurasia and Gondwana, since closure of the Paleotethys Ocean was accompanied by counterclockwise rotation of the spreading axis of the Neotethys Ocean and terrane belts. This is also confirmed by paleomagnetic studies of Jurassic and Lower Cretaceous formations of the Southern Alps region [87]. Based on a study of paleomagnetic data of Triassic rocks in a number of areas, it was assumed that during this period, the spreading axis of the Neotethys, which had previously been located in the Eastern Mediterranean region, had turned counterclockwise [87].

Tectonic–Sedimentary Analysis

Along with the modern and Late Cenozoic asymmetric grabens confined to the Dead Sea Transform (DST), more ancient structures of a similar type have been outlined in the studied region recorded according to the data of tectonic–sedimentary mapping [34]. This is an asymmetric en-echelon Paleogene trough confined to the Palmyride–Antilebanon terranes, where Paleogene deposits of the Southern Palmyrides reach the maximum known thickness within the Mesozoic terrane belt–1417 m [34]. The Late Cretaceous Azrak–Sirkhan graben, which formed in the northern part of the Neoproterozoic fold belt south of the Mesozoic terrane belt, is also a significant tectonic–sedimentary formation [34]. This asymmetric graben is distinguished by anomalously high thicknesses of the Upper Cretaceous (up to 2747 m) in the extreme eastern part, the maximum for the entire Arabian Plate. To the west, the thickness of the Upper Cretaceous over a distance of 25 km sharply decreases to 1400 m; further west, it gradually decreases to 80–600 m. The anomalous en-echelon Late Cretaceous trough of the Antilebanon and Galilea-Lebanon terranes is characterized by a similar asymmetry, respectively, which has the following thicknesses of sedimentary deposits in this zone: (i) the maximum thickness in the east of the zone up to 1453 and 1550 m and (ii) the minimum thickness in the west of the zone of 449–300 m.

Thus, the tectonic–sedimentary data on the thickness distribution of the sedimentary layer (Paleogene–Upper Cretaceous) attributed to the postaccretionary stage of the region's geological history indicate that prior to the Red Sea rifting system (Late Cretaceous–Paleogene), asymmetric and often en-echelon-like troughs were developed in the region with an anomalously high sedimentation capacity in the east of the region. The data presented show a tendency towards counterclockwise rotation of crustal blocks.

Analysis of Paleobiogeographical Data

Studies of paleobiogeographic data indicate rotation of the near-surface structures that obviously associated with the deep structure rotation.

A specific feature of the Mesozoic fauna in the Nubian–Arabian region (East Gondwana) and adjacent island arcs of the Neotethys is the development of shallow-water benthic faunal associations with increased gigantism among a number of brachiopod

Fig. 7. Tectonic–geophysical sketch map of the studied region superimposed on the gravity polynomial cubic surface approximation (approximation shown in Fig. 2). (*1*) Archean cratons, (*2–4*) fold belts: (*2*) Paleo–Middle-Proterozoic, (*3*) Neoproterozoic, (*4*) Late Paleozoic (Hercynian), (*5*) Mesozoic terrane belt, (*6*) Alpine–Himalayan orogenic belt, (*7*) Cenozoic traps of the African–Arabian rift belt, (*8*) main fault systems, (*9*) Kiama paleomagnetic hyperzone of inverse polarity [32, 34], (*10*) isolines of the obtained polynomial regional gravity trend, (*11*) depth of epicenters of the deep-focus earthquakes: (*a*) 150–300 [30, 49, 119, 125], (*b*) 300–600 [30, 49, 119, 125], (*c*) >600 km [30, 49]; (*12*) rotational geodynamic elements derived from: (*a*) paleomagnetic (major) and tectonic (minor) data: (**1**) Piennine klippen belt (West Carpathians) [82], (**2**) Getic Basin (South Carpathians–Moesia) [75], (**3**) Athos Peninsula (Greece) [72], (**4**) Samothraki (Greece) [72], (**5**) Crete (Greece) [28], (**6**) Menderes massif (western Anatolia, Turkey) [115], (**7**) Cyprus [16, 17], (**8**) Kiama paleomagnetic hyperzone (Eastern Mediterranean) [32, 34], (**9**) Galilee (Israel) magmatic and block systems [15, 96], (**10**) dikes of Makhtesh Ramon (Negev terrane, Israel) [34], (**11**) block systems of Gulf of Aqaba (northern Egypt) and Midian fault zone (far west of Saudi Arabia) [8, 11], (**12**) dikes of Sinai Peninsula [57], (**13**) block system of Sinai Bay [19], (**14**) bottom deposits of northern Red Sea [8], (**15**) Mansouri ring complex (SE Desert, Egypt) [78], (**16**) Barake suture zone (Red Sea) [80], (**17**) northeast of Afar Depression (Eritrea) [86], (**18**) central part of Galilee–Lebanon terrane [55], (**19**) Eastern Taurides [56, 84], (**20**) seismotectonic shear zone (Black Sea, southern Crimean Peninsula) [20], (**21**) Rioni Basin (Georgia) [9, 56], (**22**) Eastern Pontides [56, 94], (**23**) Achara–Trialet belt (Georgia) [94], (**24**) Dagestan Mountains (Eastern Caucasus) [51], (**25**) Kur Depression [52, 58], (**26**) Somkheto-Garabakh belt [69, 70, 90], (**27**) Nakhichevan and Talysh regions (Azerbaijan) [51, 94], (**28**) Kata-Rash area (Iraq) [34, 35], (**29**) foot of Mt. Hermon (northern Israel) [122], (*b*) GPS constructions, with generalization [27, 91]. SF, Sinai Fault; DST, Dead Sea Transform; MEEF, Main Eastern European Fault; EMNB, Eastern Mediterranean Nubian Belt; OF, Owen Fault; WC, Western Caucasus; EC, Eastern Caucasus.

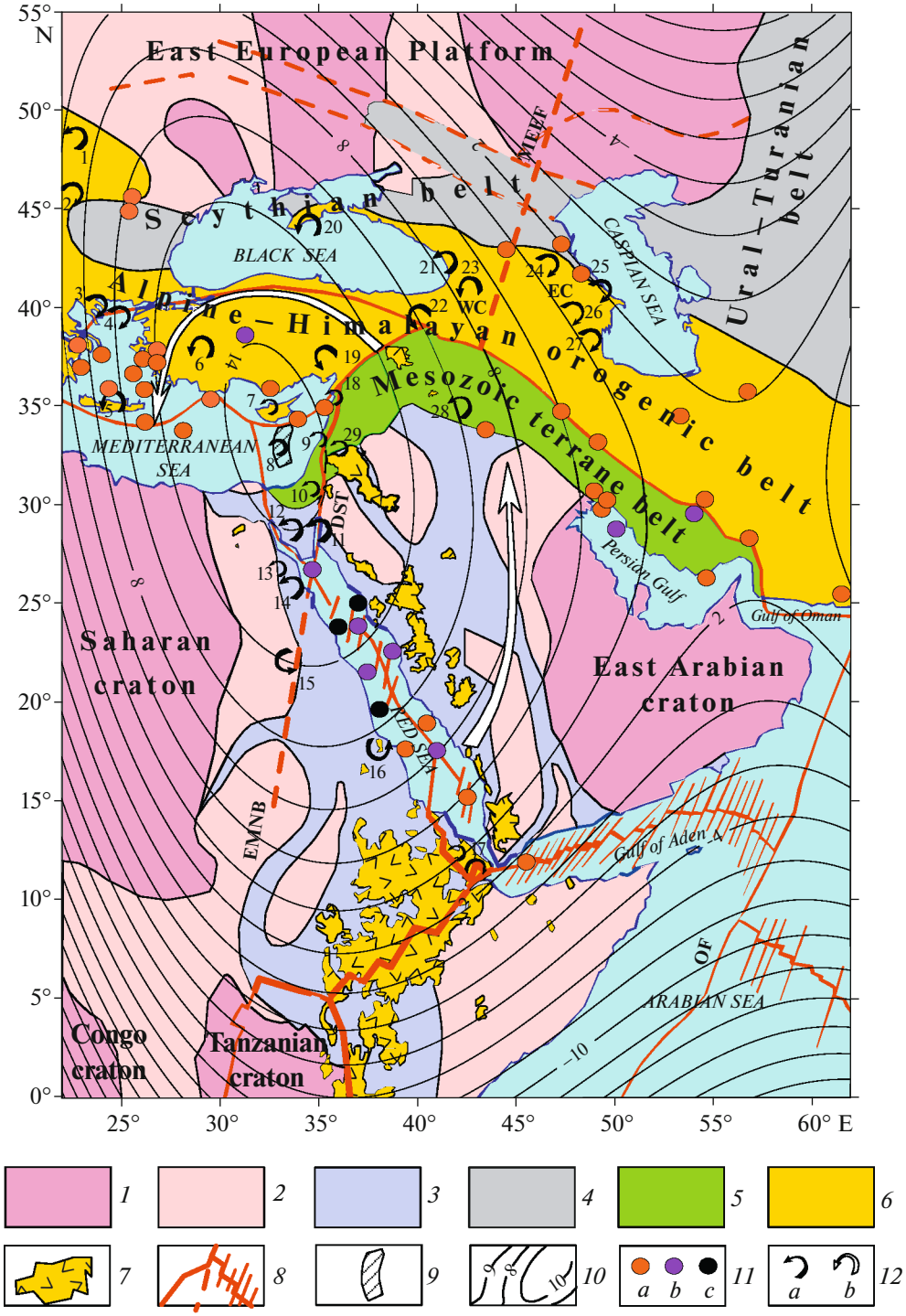

and mollusk groups. First, these are the identified Middle Triassic myalinid bivalves *Ramonalina ramanensis*, which reached a length of up to 15 cm, the largest bivalve mollusks of all found so far in the world in Middle Triassic sediments [123]. Finds of this unique fauna are known in the Negev terrane (southern Israel). Structurally and tectonically, the terrane is allochthonous; it was displaced by hundreds of kilometers from the island arcs of the southern frame of the Neotethys to the western segment of the present Eastern Mediterranean region [34]. Further biogeographic data on Jurassic and Cretaceous fauna are more numerous and have been systematized for use in tectonic–paleogeographic analysis. Therefore, we do not consider all data, but only those on development of the most important biogeographic indicators.

The Late Jurassic shallow-water sediments of the Negev, Antilebanon, and northern and southern Palmyride terranes include coral biostromes with abnormally large brachiopod shells and sea urchin spines. The brachiopod fauna (*Somalirhynchia–Septirhynchia*) in these facies directly resembles the studied facies of the Ethiopian biogeographic province of Saudi Arabia, Ethiopia, and Somalia [34]. Thus, the sedimentary deposits of foreland of the Northern Arabian and Eastern Nubian regions show a tectonically discordant relationship with the allochthonous Mesozoic terrane belt (Fig. 7), which rotated counterclockwise towards Gondwana.

This proves the counterclockwise movement of the eastern and central parts of the near-surface projections of the deep structure in the Jurassic and Early Cretaceous. For the first time, this makes it possible, using geodynamic and geophysical characteristics, to explain the uniqueness of the biogeographically anomalous zone of terrane blocks accreted to Gondwana in the mid-Early Cretaceous, during the Levantine phase of tectogenesis.

The next unique paleobiogeographic phenomenon, still unexplained, is the final phase of the fauna of the giant brachiopods *Praeneothyris* in the Late Cretaceous in the territory stretching from the Hindustan Plate (Southeast India, state of Madras) to the boundary regions of Paleozoic and Mesozoic–Cenozoic consolidation of Central Asia—rom the Tajik, Fergana depression (Tajikistan, Uzbekistan) to Gorny Badkhyz (Turkmenistan), the South Aral part of the Turgai Plate (Uzbekistan); and further to the west—from the Mesozoic–Cenozoic consolidation of the Lesser Caucasus to the Bulgarian Paleozoic part of the Rhodope massif [3, 63]. The absence of such fauna in the nearby Balkanides terrane belt most likely indicates the allochthonous nature of accretion of the terrane block group in the Rhodope zone, geodynamically similar to the Early Cretaceous Levant terrane belt which contains the Ethiopian fauna. Thus, two important biogeographic anomalous belts have been delineated: (i) Jurassic with *Somalirhychia–Septirhynchia*, and (ii) Late Cretaceous with *Praeneothyris*. These biogeographically anomalous belts have been allochthonously displaced to the west as a result of the movement of crustal block structures counterclockwise both in the zone of the central part of the projection of the deep structure on the subsurface section located near Gondwana, and in the more northern zone confined to a complex system of rift basins and terrane blocks of the mobile belt of the Neotethys Paleocean systems.

Analysis of Asymmetric Basins in the Region

Ben-Avraham [12] and Smit et al. [103] studied the development of asymmetric basins along transforming continental faults in the eastern part of the surface projection of the revealed deep structure. We assume, in light of our data, that the asymmetric structure of these basins and their left-lateral regional counterclockwise rotation were influenced by the deep structure.

In the Gulf of Aqaba, three deep-water trough systems have developed from south to north. They are shifted from east to west and form a series of en-echelon troughs. The similar arrangement of the structures suggests that not only a shear mechanism prevails here, but also counterclockwise block rotation.

In the Dead Sea region, as well as in the Eilat (Israel–Jordan) graben system, the axial part of the graben is confined to the east, while the flattened part of the structure extends to the west [11, 12, 44]. The tectonic–geomorphological and magmatic asymmetry of the eastern and western coasts of the Dead Sea basin is well known, while the eastern part of the basin has a higher amplitude and is more active [44].

Based on the general gently arcuate structure of the DST [103], we have proposed a new geodynamic concept to explain the asymmetry of the tectonotype of the deep displacement of the grabenlike structures. Its essence is the regional development of not only shear, but also rotational displacements of crustal blocks, which we consider the basic position for explaining the asymmetry of the regional basins.

The Sea of Galilee (Lake Kinneret) is located on the northern continuation of the DST in northern Israel. It has long been known that the axis of the deep-water basin of Lake Kinneret was displaced to its eastern shore, while the axis of its shallow-water basin was displaced to the western shore [31]. A model of tectonic shear along a line or system of transform fault lines was proposed earlier [12]. However, analysis of paleomagnetic data [96] obtained from areas adjacent to the Galilee region, as well as structural mapping data have revealed widespread arcuate faults in the shear zone [103], allow us to clarify the general dominant nature of the geodynamics of regional movements. They are combined with counterclockwise axial rotation of the continental crustal blocks of the Arabian–Nubian region, which agrees well with the GPS monitoring data.

The asymmetry of local sedimentary basins in the area of the projection of the deep structure is also emphasized by the features of geomorphological asymmetry of the Arabian–Nubian zone of Gondwana in the Late Cenozoic. In its western part, corresponding to the junction of the Nubian Plate and the Red Sea rift zone, the hypsometric marks of the plateau and Nile River valley developed here generally do not exceed 500 m. In the eastern part (Arabian–Sinai zone) of the junction of these lithospheric plates with the Red Sea rift zone system and Dead Sea shear zone, the hypsometric marks clearly exceed 500–1000 m (Fig. 1). In the marginal zones of the Arabian and Sinai plates, mountain ranges with heights of more than 2000–3000 m have formed. We suggest that the described phenomenon of regional

geomorphological asymmetry of the two sides of the Red Sea rift zone is geodynamically determined by the counterclockwise rotation of the region.

Deep Seismic Tomography

The presence of the giant deep quasi-circular structure in the lower mantle beneath the Eastern Mediterranean is also confirmed by the results of deep seismic tomography [99, 109, 117, 118, 121], which indicate anomalous velocities of P- and S-wave propagation at depths of 1200–1800 km. Van der Meer [118] presented a seismic tomographic profile through the Antalya region at 40° N (southern Turkey). Here, seismic tomography data (plotted from both P- and S-waves) indicate the presence of a heterogeneous anomalous source in the mantle within the contour of the giant deep ring structure [118]. Here, in the rotating circular (elliptical) structures with inhomogeneous composition, anomalous processes of different signs can occur [2].

Analysis of Paleomagnetic Data

Paleomagnetic data were analyzed out mainly for Cenozoic and partly Upper Cretaceous rocks. The study of the geodynamics of the central part of the projection of the deep anomalous ring structure (including the structural zones of the Eastern Taurides, Cyprus arc, southern and northern margins of the Mesozoic terrane belt, and western margin of the Neoproterozoic fold belt) indicates that the rotation of tectonic blocks is predominantly counterclockwise (Fig. 7) [16, 34, 55, 69, 71, 78]. In the structure of the Western Caucasus, attributed to the peripheral part of the projection of the deep structure, dominant counterclockwise rotation of blocks is observed, while in various structural zones of uplifts and troughs of the Eastern Caucasus located outside the contour of the deep mantle structure, clockwise rotation of the crustal blocks has been revealed [9, 51, 52, 56, 69, 94] (Fig. 7).

Studies of paleomagnetic data in the western, peripheral part of the projection of the deep structure, in the junction zone of various tectonic structures and blocks, from the arc of the Western and Southern Carpathians, the Hercynian Rhodope massif to the arcs of the Pelagonian zone and the Hellenides, extending into the Aegean Sea basin, show geodynamic instability. In particular, this follows from the data on identification of neotectonic movements of the northern and southern sides of the Aegean Sea. Paleomagnetic studies of the North Aegean granitoids and volcanic rocks (island of Samothraki and the Athos Peninsula in northeastern Greece), according to [72], indicate clockwise rotation of this region, which is attributed to the Rhodope massif of the Eurasian Plate.

Meanwhile, most of the data obtained for the region in the central and southern parts of the Aegean Basin [81] and particularly in Crete [28], show a tendency towards counterclockwise rotation in the Late Cenozoic. Similar instability in the rotation of various tectonic blocks is also manifested in the Carpathian fold region. In the north, within the inner belt of the Piennine klippes of the Western Carpathians, the blocks were found to rotate counterclockwise [82], while the South Carpathian Gothic Basin of Moesia rotates clockwise [75].

These paleomagnetic rotations agree with the configuration of the polynomial gravitational anomaly (Fig. 2), geoid anomalies (see Fig. 4), and the distribution of GPS vectors (Fig. 4).

Morris et al. [85] found that rocks of the Troodos (Cyprus) and Baer-Bassit (Syria) ophiolite massifs underwent significant counterclockwise rotation. Paleomagnetic reconstructions made it possible to compile visual geodynamic diagrams illustrating the counterclockwise rotation of the structure of Cyprus from the Cretaceous to the Late Cenozoic (Fig. 8).

Paleomagnetic Hyperzone Kiama and Ancient Oceanic Crust

The central part of the projection of the deep structure (central part of the Eastern Mediterranean) is also associated with anomalously low regional heat flow values (~15–30 mW/m^2) [5, 29, 34], which we consider a reflection of the ancient age of the lithosphere in the studied region. Low heat flow values also indicate a cooling lithosphere. The uniqueness of this zone is emphasized by the discovery (based on the combined analysis of different geological–geophysical data) of one of the most ancient blocks of oceanic crust, attributed to the Kiama paleomagnetic hyperzone of reverse polarity (Late Carboniferous–Early Permian) [32].

The upper edge of this block lies at a depth of about 10–11 km at the center of the projection of the deep structure, a few tens of kilometers south of Cyprus [32, 34] (Fig. 7). The initial formation of the Kiama hyperzone [34] could have occurred east of the current position of the Persian Gulf [53]. This tectonic block apparently moved along regional transform faults to its present position, influenced by counterclockwise rotation of the projection of the deep structure. It can be suggested that the decisive influence of the deep structure just prevented the subduction of this oceanic block and preserved its location to the present.

Position of the Mesozoic Terrane Belt

One of the most important element of the regional structure of the Near East determining the geodynamic processes and tectonics of this complex region is the Mesozoic terrane belt, discovered in [10, 13, 14] and thoroughly investigated in [34, 36, 38] (Fig. 7).

Until the early 1990s, in all paleogeographic and tectonic maps, the region of the Eastern Mediterranean was attributed to the Precambrian Arabian Plat-

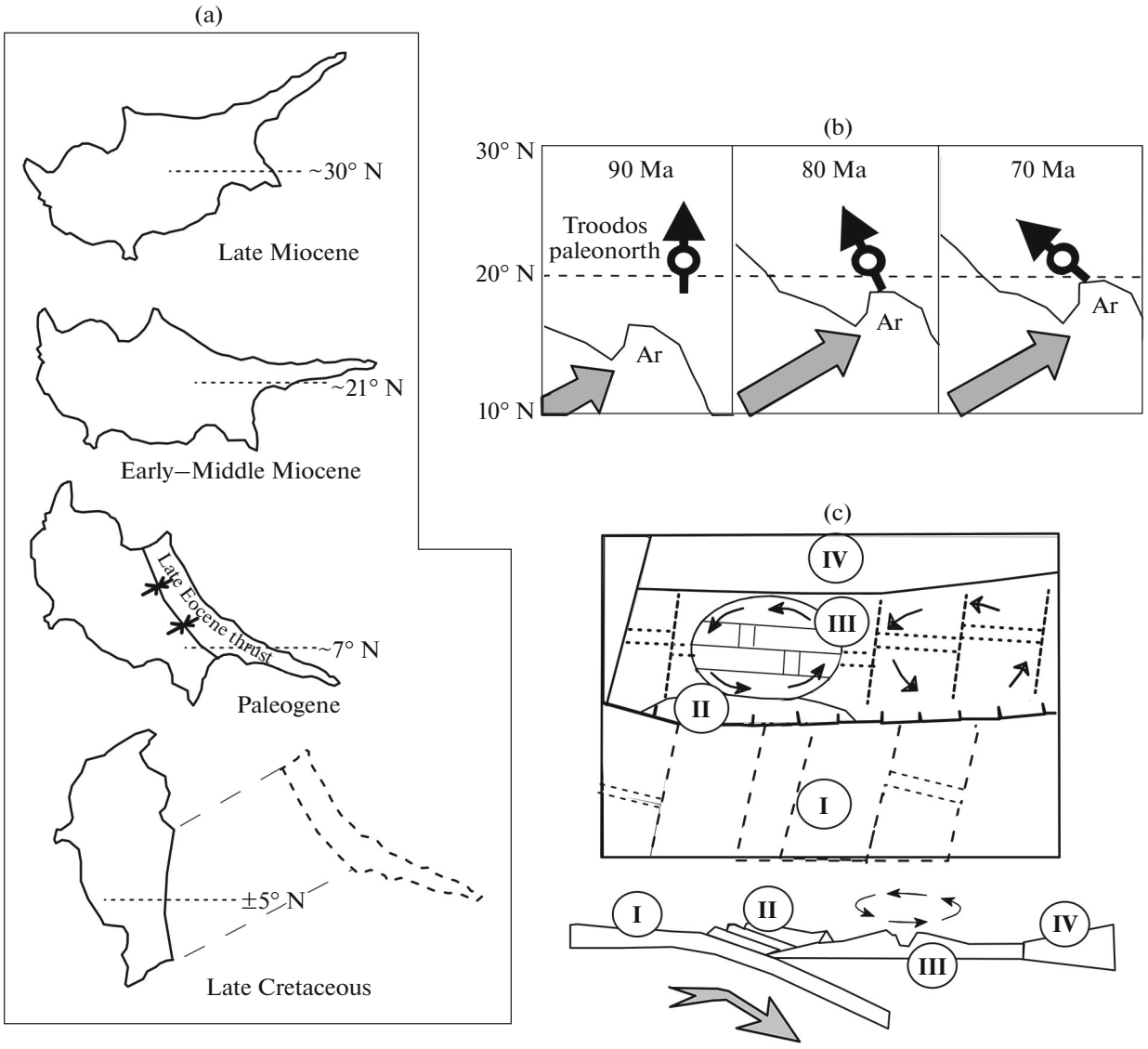

Fig. 8. Geodynamic schemes of rotation of structure of Cyprus (Cretaceous–Late Cenozoic) (a) counterclockwise rotation of Cyprus from Late Cretaceous to Late Miocene (according to paleomagnetic data [16]), (b) change in relative position of Cyprus and the African–Arabian Plate of Gondwana paleocontinent in Late Cretaceous (according to paleomagnetic data [85]), (c) structural–paleogeodynamic reconstruction of paleostructures of Cyprus within Late Cretaceous Tethys Paleocean and its frame (after [53]). I, subducting oceanic plate of southern side of Neotethys; II, ophiolite complex of Early Mesozoic crust of Mammonia basin; III, area of spreading zone of Late Cretaceous part of middle Troodos ridge; IV, zone of terranes of the Aegean–Anatolian belt with continental crust.

form (e.g., [13]), complicated in the western part by a deep left-lateral shear including a system of grabenlike troughs and called the DST. The frontal part of the Precambrian Platform, which has a fold-block structure, was called the Syrian arc (arch), the age of which was considered Late Cenozoic. It was also assumed that movements of the platform were due to peculiarities in the geodynamics of the DST or even the influence of trans-African faults stretching west from the Atlantic Ocean [53].

Having carried out a study of the thicknesses, velocities, and geodynamic features of the crust of various zones and structures of the Eastern Mediterranean, Ben-Avraham [10, 13, 14] showed for the first time that the dominant tectonic evolution model for this region was not rifting caused by Late Cenozoic spreading of the Red Sea system, but earlier collision of the terrane blocks associated with closure of the Neotethys.

However, it became obvious that these propositions should be supplemented by numerous regional stratigraphic, paleogeographic, facies, biogeographic, geomorphological, tectonic–sedimentary, petrological, mineralogical, radiometric, and tectonic data revealed from studying both surface landforms and cores from numerous deep boreholes. This allowed us to generalize the results of a large number of detailed

geological surveys and compile new paleogeographic, paleomagnetic, and tectonic–geophysical maps for this region [32–38].

Geological–Geophysical Characteristics of the Mesozoic Terrane Belt

We have presented the most important aspects and geological–geophysical characteristics of the Mesozoic terrane belt (Fig. 7) essential for substantiating the deep mantle structure that influenced the features of its formation. The data of the tectonic–sedimentary analysis indicate that in the Jurassic–Cretaceous, these terranes differed from each other and from the foreland troughs associated with the passive margin of the Neotethys, since they are tectonically discordant. Biogeographic data (development of Jurassic fauna of the Ethiopian province in these terranes) indicate their allochthonous (eastern) origin, which according to the paleogeographic data could be a continuation of the shelf gulf of northeastern Arabia, i.e., at a distance of 500–1000 km from the current location of the terranes. Tectonic–sedimentary maps of the Eastern Mediterranean compiled for the Lower and Upper Cretaceous, Paleogene, and Neogene–Anthropogene showed the autochthonous occurrence of all rocks except for a neotectonic displacement of 100 km along the DST [44].

The compiled paleogeographic map of the Lower Cretaceous shows that during erosion of the consolidated terrane belt of Triassic and Jurassic formations underlying the regional unconformity surface, erosion cuts with amplitude of washout of up to 1000–1200 m were formed [34]. The radiometric age of this unconformity determined from collision traps in the Atlit-1 well (this parametric well was drilled under the patronage of the Israel Geological Survey in the Atlit settlement on the Mediterranean coast in the northern Israel) is about 133 Ma, which corresponds to the identified Levantine phase at the boundary of the Lower and the Upper Hauterivian [34].

Terranes of this belt have moved westward in a counterclockwise direction at an earlier time—during the Late Jurassic and beginning of the Early Cretaceous. This phenomenon was determined by the radiometric age and direction of rotation of precollisional traps–numerous basaltic dikes of the Makhtesh Ramon erosion–tectonic depression in southern Israel [35].

In the Mesozoic terrane belt (see Fig. 7), the presence of terranes was revealed [10, 13, 14], but only identification of the Levantine phase as the main collisional stage of this terrane belt's accretion to Gondwana made it possible to determine its Mesozoic age. Therefore, this terrane belt was classified as a fold-block belt with Mesozoic consolidation [34] (Fig. 7).

The most significant geodynamic factor of the Mesozoic terrane belt (Fig. 7) is the movement of its structural elements during the Jurassic and Early Cretaceous along a series of transform faults for up to 1000 km in the counterclockwise direction to the Eastern Mediterranean (as we assume, under the influence of the deep mantle structure). In the process of these movements, ancient oceanic crust of the Neotethys, together with the Kiama paleomagnetic hyperzone zone, was entrained and moved in the same direction [37].

GENERALIZED GEOLOGICAL–GEODYNAMICAL ANALYSIS

The integrated geophysical–geodynamic-geological map in Fig. 9 shows a number of geodynamic indicators: the position of GPS vectors and numerous geological indicators: outcrops of deep magmatic elements and the main tectonic features of the region [6, 26, 35, 40, 41, 50].

Outcrops of various deep-seated magmatic elements in Cyprus indicate a high level of tectonic–geodynamic activity in the near-surface projection of the deep anomalous zone [21, 48, 110]. The distribution of GPS vectors (see Fig. 4), which clearly shows counterclockwise rotation, agrees well with the isolines of the regional gravitational trend (Fig. 2) and indicates the presence of the so-called geodynamic vortex structure in the central-western part of the region. At the center of this structure, the Cyprus high-amplitude gravitational anomaly occurs [27, 46, 91] (Fig. 6). However, outside the contour of the gravitational trend, e.g., in the northeast of the region, the GPS vectors gradually acquire a clockwise direction (Fig. 4). This phenomenon in the aforementioned area is also accompanied by changes in the direction of paleomagnetic vectors from counterclockwise to clockwise (Fig. 7).

In tectonic–magmatic terms, the noted regional asymmetry of the Red Sea Basin is even more pronounced. Most dike complexes of the Oligocene–Early Miocene intrusive traps marking the formation of the Red Sea rift zone have developed on its Arabian coast and in Sinai (east of the Suez graben). Younger, more extensive spots of Middle Miocene–Pleistocene effusive traps are widespread east of the strip of dikes continuing and turning counterclockwise further northward to the Pannonian massif of Transcarpathia (Fig. 10) and further along an arc to the south—to the area of a significant magmatic node—the explosive Santorini volcano. This volcano, which is located near the critical 35° N and the projection of the center of the deep anomalous structure onto the surface, was the basis of one of the most significant geocatastrophes in world history (17th century BCE).

We have identified two linear belts (Cretaceous and Late Cenozoic) characterized by counterclockwise rotation, but differing in age and nature of magmatism [36]:

(1) The Cretaceous belt has a variety of magmatism with a wide development of alkaline and kimberlite associations marked by finds of diamonds and their

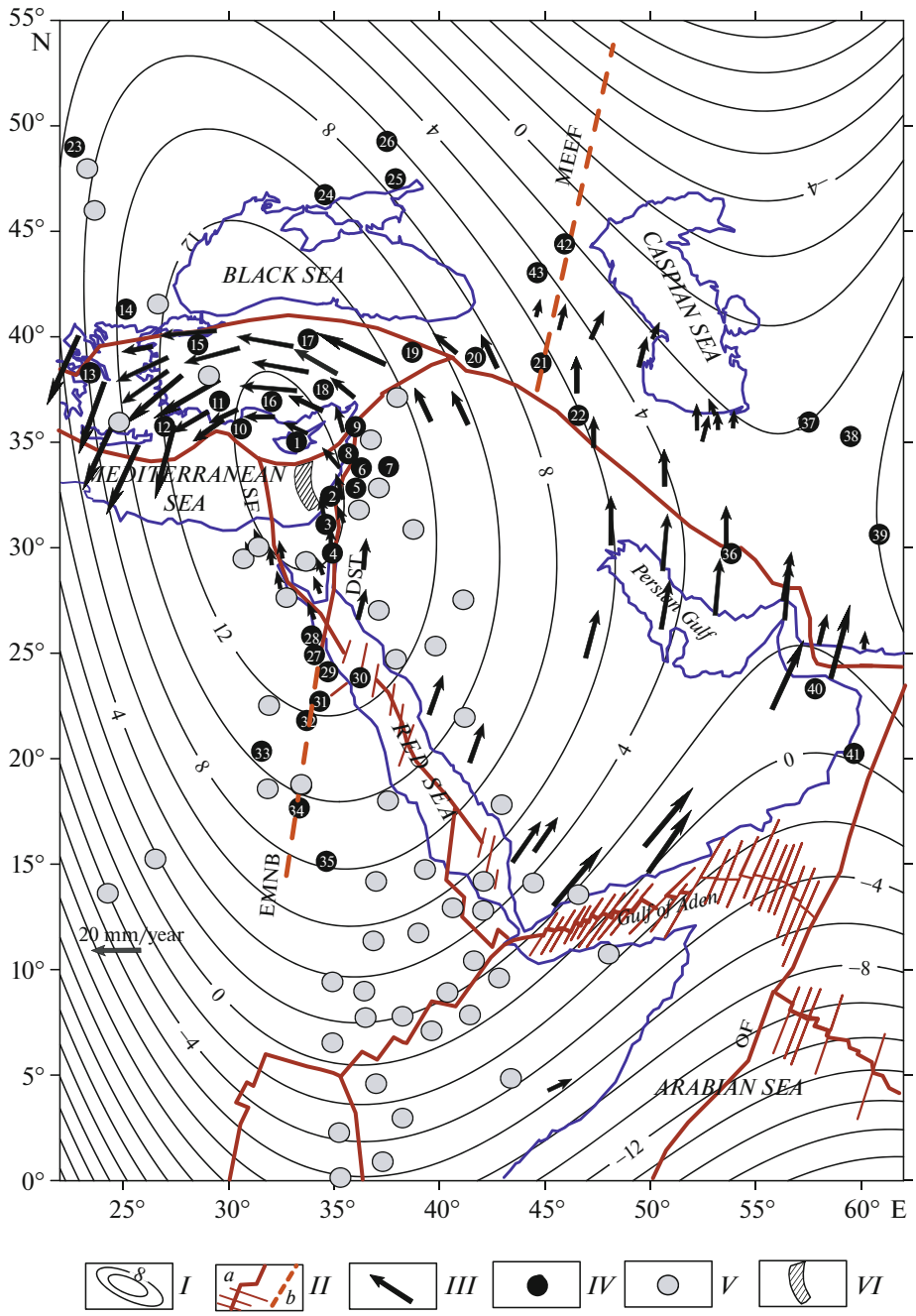

accessory minerals–from northern Syria to Egypt's Eastern Desert [6, 40, 50, 100].

(2) The Late Cenozoic belt is predominantly composed by a thick trap association, and the most ancient part of it corresponds to the boundary between the Eocene and Oligocene in the Afar hotspot area, and extends in the form of comparatively small spots to the Pannonian massif of Transcarpathia.

These two linearly elongated belts of the Mesozoic and Cenozoic magmatism (which intersect each other) mark the spatial movement of the deep mantle structure relative to the crust and mantle lithosphere. They represent axial lines of different ages through the deep-seated magma- and ore-controlling faults intersect various geotectonic zones of the crust. Obviously, the Red Sea rifting zone is part of a continuous deep fault, which continues northward to the Carpathian region and intersects different structures and lithospheric plates. This fault coincides with the projection of the long axis of the deep mantle structure.

The central (apical) part of the deep mantle structure forms the Sinai Plate bounded meridionally by two faults. In the north, the Sinai Plate is bounded by

Fig. 9. Integrated geological–geophysical diagram of geodynamic indicator distribution in the study region (superimposed with the obtained polynomial gravity trend from Fig. 2). Corresponding references for (IV) are presented in [37]. (*I*) Isolines of gravitational trend (see also Fig. 2), (*II*) faults: (*a*) main interplate, (*b*) main intraplate; (*III*) GPS monitoring vectors [27, 91]; (*IV*) most significant outcrops with Mesozoic mantle rocks and minerals (numerals in circles): (1) Troodos ophiolites (Cyprus), (2) basalts of Mt. Carmel (northern Israel), (3) alkaline rocks of Makhtesh Ramon tectonic–erosion depression (southern Israel), (4) basitic rocks of Timna volcanic depression (southern Israel), (5) Jebel Sheqif traps (western Lebanon), (6) Nabi Matta intrusions (northwestern Syria), (7) Jebel Rmah traps (western Syria), (8) Baer-Bassit ophiolites (northwestern Syria), (9) Kizildag ophiolites (southern Turkey), (10) Antalya ophiolites (southwestern Turkey), (11) Lycian ophilotes (Turkey), (12) Karfatos-Rhodes ophiolites (southern Greece), (13) Locris-Beotia ophiolites (central Greece), (14) Krumovgrad alkaline basalts (southern Bulgaria), (15) Harmanchik ophiolites (northwestern Turkey), (16) Beysehir ophioltes (western Turkey), (17) Ankara ophiolite mélange (northern Turkey), (18) Pozanti-Korsanti ophiolites (southern Turkey), (19) Tunceli ophiolites (southeastern Turkey), (20) Guleman ophiolites (eastern Turkey), (21) Khoy-Maku ophiolites (northwestern Iran), (22) Kermanshah–Kurdistan ophiolites (northeastern Iraq–northwestern Iran), (23) Sedlice peridotites (eastern Slovakia), (24) Lake Sivash traps (southern Ukraine), (25) alkaline dikes of Azov massif (southern Ukraine), (26) Izium tuffaceous rocks (eastern Ukraine), (27) Abukhruq alkaline traps (southeastern Egypt), (27a) Afia kimberlites, Wadi Zediun [(southeastern Egypt), (28) El Kahfa alkaline traps (southeastern Egypt), (29) Zabargad Island peridotites (Red Sea, Egypt), (30) El Naga alkaline traps (southeastern Egypt), (31) Mansouri alkaline traps (southeastern Egypt), (32) Delgo volcanics (northern Sudan), (33) Wadi Shaq Um Bosh alkaline traps (eastern Sudan), (34) Mindara alkaline traps (eastern Sudan), (35) Neyriz ophiolites (southeastern Iran), (36) Sabzevar ophiolites (northern Iran), (37) Torbat-e-Haidarieh ophiolites (northeastern Iran), (38) Birjand-Nehbandan ophiolites (eastern Iran), (39) Semail ophiolites (Oman), (40) Masirah Island ophilolites (Oman), (41) Svetloyar traps, Stavropol uplift (southwestern Russia), (42) Kuban traps (northwestern Caucasus, Russia). (*V*) Late Cenozoic traps, (*VI*) Kiama paleomagnetic hyperzone (Eastern Mediterranean) of reverse polarity [22]. SF, Sinai Fault; DST, Dead Sea Transform; MEEF, Main Eastern European Fault; EMNB, Eastern Mediterranean Nubian Belt; OF, Owen Fault.

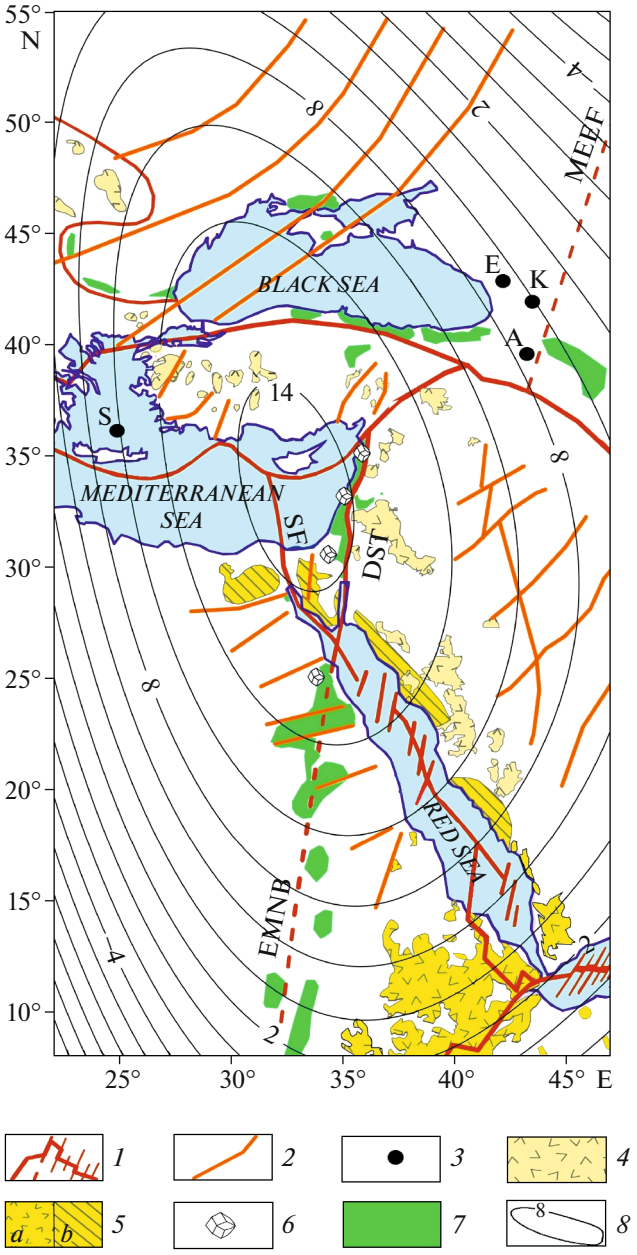

Fig. 10. Cretaceous (Mesozoic) and Late Cenozoic magmatic and disjunctive indicators of deep mantle structure in zone of the Eurasia and Gondwana junction: (*1*) major interplate and intraplate deep faults, (*2*) deep faults caused by modern geodynamic activity [45, 105, 108] of mantle structure, (*3*) largest volcanoes of central type and calderas: A, Ararat; E, Elbrus; K, Kazbek; S, Santorini; (*4*) zones of development of Neogene–Quaternary effusive traps [25, 81]; (*5*) zones of development of Oligocene–Miocene: (*a*) effusive traps, (*b*) dike complexes; (*6*) points of diamond discovery according to [6, 40, 50, 100]; (*7*) zones of development of Cretaceous traps and island-arc magmatic complexes [24, 34, 54, 89, 92, 116]; (*8*) isolines of regional gravity trend.

a fault that develops from the southern part of the Aegean–Anatolian Plate. The southern part of Cyprus with the development of a Cretaceous mantle diapir (which reaches out the surface), adjoins the zone of the Eastern Mediterranean oceanic terrane, which is characterized by the oldest oceanic crust corresponding to the Kiama hyperzone.

Peripheral tectonic–thermal and geodynamic processes following from analysis of this map (Fig. 10) also require commentary, since rather large-scale processes and structures are manifested here. First of all, these are the large volcanoes Elbrus, Kazbek, Ararat, Demavend, Kenya stratovolcano, the Afar triple junction, and the Santorini volcano caldera formed by hot spots distinctly located on the periphery of the projection of the deep mantle structure (Fig. 10). It can be suggested that this combination is random. However, let us analyze the location of these volcanoes together with GPS data, transformants of satellite gravimetric

data, the seismicity of the Vrancea zone, and series of deep suprastenospheric faults extending from it, which penetrate deep into the zone of the central part of the East European Precambrian Platform. Integration of these factors allows a conclusion on the regularity of the phenomena caused by the influence of the deep structure.

The unique development of the Arabian Late Cenozoic effusive traps has been substantiated tectonically by Kazmin's regional geodynamic model [65], which outlined the development of regional shear and interlayer breaking of the thinned lithosphere during the formation of the Red Sea rift. Later it was confirmed by the authors of this article [37].

The map of the total thickness of the lithosphere (Fig. 11) shows that the general minima of the thickness coincide with the rift zones of the Red Sea, the Gulf of Aden, and, partially, East Africa. They outline not only large plates–the Arabian, Nubian, Somali, and southern margins of the Eurasian Plate—but also smaller plates–the Sinai and Victorian. Thickening of the lithosphere in the central part of the Sinai Plate is explained by presence of a frontal zone of the Mesozoic terrane belt with developed ophiolite and subduction complexes of the oceanic crust of the northwestern margin of the Neotethys [35]. Our data indicate the geodynamic asymmetry between the eastern and western coasts of the Red Sea. Thickening of the mantle lithosphere is displaced to the east in the direction of counterclockwise rotation of its deep structure to the central region of the Arabian Plate, with a maximum thickness of ≥150 km in the frontal zone of deep movement of masses. The thickness minima (~70–75 km) outline the eastern coast of the Red Sea and the zone east of the DST, where the Late Cenozoic traps are developed.

The thinned lithosphere of the western coast of the Red Sea is characterized by the underdeveloped Late Cenozoic trap magmatism and rather distinct deep-seated Cretaceous and Triassic alkaline magmatism [116]. The lithosphere of the region reflects both thinning of the crust and the mantle lithosphere of the Late Proterozoic belt with the transitional regime that developed here, as well as the presence of a relict Mesozoic axial zone of the deep mantle structure with active Cretaceous magmatism to the north, in the zone of the later DST, and further, in the Neotethys.

Thus, the map of crustal and upper mantle thicknesses (Fig. 11) reflects the following geological and geophysical aspects of the dynamics of the projection of the deep structure:

(1) a clearly pronounced tendency toward counterclockwise axial rotation of deep masses of the mantle lithosphere with a thickening of the frontal part of the moving masses,

(2) thinning of crustal-mantle masses in the axial part of the deep structure at the modern stage of Late Cenozoic spreading,

(3) the presence of a relict zone of thinning of the axial lithosphere of the Mesozoic axis of projection of the deep mantle structure discordantly located with respect to the spreading axis of the Neotethys.

This explains the uniqueness in the similarity of structures and the nature of cyclicity of Cretaceous trap magmatism of the Gondwana Mesozoic belt and its northeastern counterparts that developed in the terrane belt of the northern margin of the Neotethys—in the Lesser Caucasus and terranes and massifs of Anatolia.

The Main East European Fault (MEEF) [73, 101] (we consider this fault as a system of faults) separates the Western and Eastern Caucasus (Figs. 7, 9). We believe that the continuation of the MEEF to the south is the East Mediterranean–Nubian Belt (EMNB) [6, 34, 37], since it is displaced relative to the MEEF by 500–600 km to the west. Presumably, the East Mediterranean–Nubian belt was an axial fault in the projection of the deep mantle structure onto the Earth's surface in the Mesozoic era (Figs. 7 and 9).

Generalization of deep mineral-petrological and tectonic–geodynamic features of the region indicate that (see Figs. 7, 9):

(1) many different manifestations of magmatism are observed in the projection of the deep structure;

(2) the largest number of occurrences of rocks and minerals of deep origin are concentrated in the apical part of the projection of the deep mantle structure, in the center of which were discovered the Cyprus ophiolite zones, where numerous mantle minerals (e.g., melilite, clinopyroxene, amphibole, olivine, Cr-spinels) were found [21, 48];

(3) the belt of Cenozoic traps along the line corresponding to the strike of the Red Sea [19] is consistent with the current position of the long axis of the projection of the deep mantle structure;

(4) the ancient axis of the projection of the deep structure is expressed by the EMNB and possibly its northern continuation—the MEEF (Fig. 7). The latter fault divides the Caucasus into its western and eastern parts;

(5) the ancient Mesozoic axis (along the East Mediterranean–Nubian belt) and the modern Cenozoic axis (along the Red Sea strike) were activated in the Late Cenozoic; they are at an angle of 35°–40° to each other and outline the western and eastern boundaries of the Sinai Plate, which was formed at the Miocene/Oligocene boundary.

DISCUSSION

The analysis of geodynamic and geological indicators for the study region was based on research of the distribution of deep magmatic elements, including ophiolites, traps, large volcanic structures and diatremes (see Fig. 9). Mesozoic outcrops (see Fig. 9) indicate location of rocks and minerals associated with the mantle inflows (ophiolites, traps, and mantle diapirs).

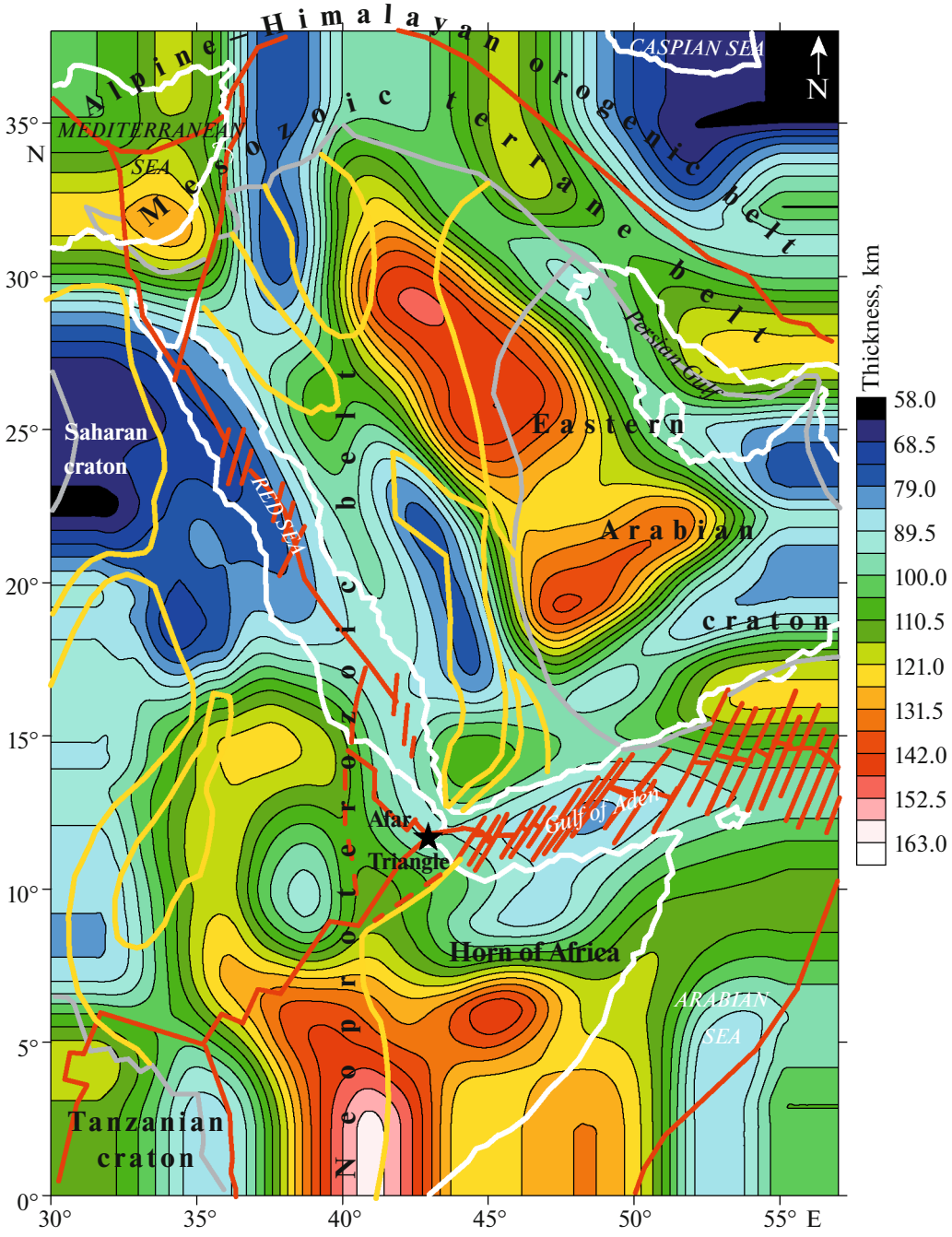

Fig. 11. Map of thicknesses of lithosphere and location of major tectonic elements (after [38], with modifications). Red lines indicate fault systems; gray lines show boundaries of cratons and tectonic belts; yellow lines show boundaries between zones of Early and Late Proterozoic consolidation and Neoproterozoic belt; white lines show boundaries between land and marine areas.

The spatial position of these indicators shows a good correlation both with the map of polynomial gravitational anomalies (see Fig. 2) and location of the GPS vectors (Figs. 4, 9).

The generalized geoid anomaly map (see Fig. 4) represents a large quasi-ring anomaly that correlates well with the polynomial gravitational anomaly map (Fig. 2), residual gravitational anomalies from the lower mantle (Fig. 3), and GPS vector distribution (Figs. 4, 9).

Both the paleomagnetic data (Fig. 7) and paleomagnetic sketch maps (Fig. 8) unambiguously indicate counterclockwise rotation of the central part of the projection of the deep quasi-ring structure. At the same time, geodynamic instability arising in the peripheral areas of the projection of the deep structure

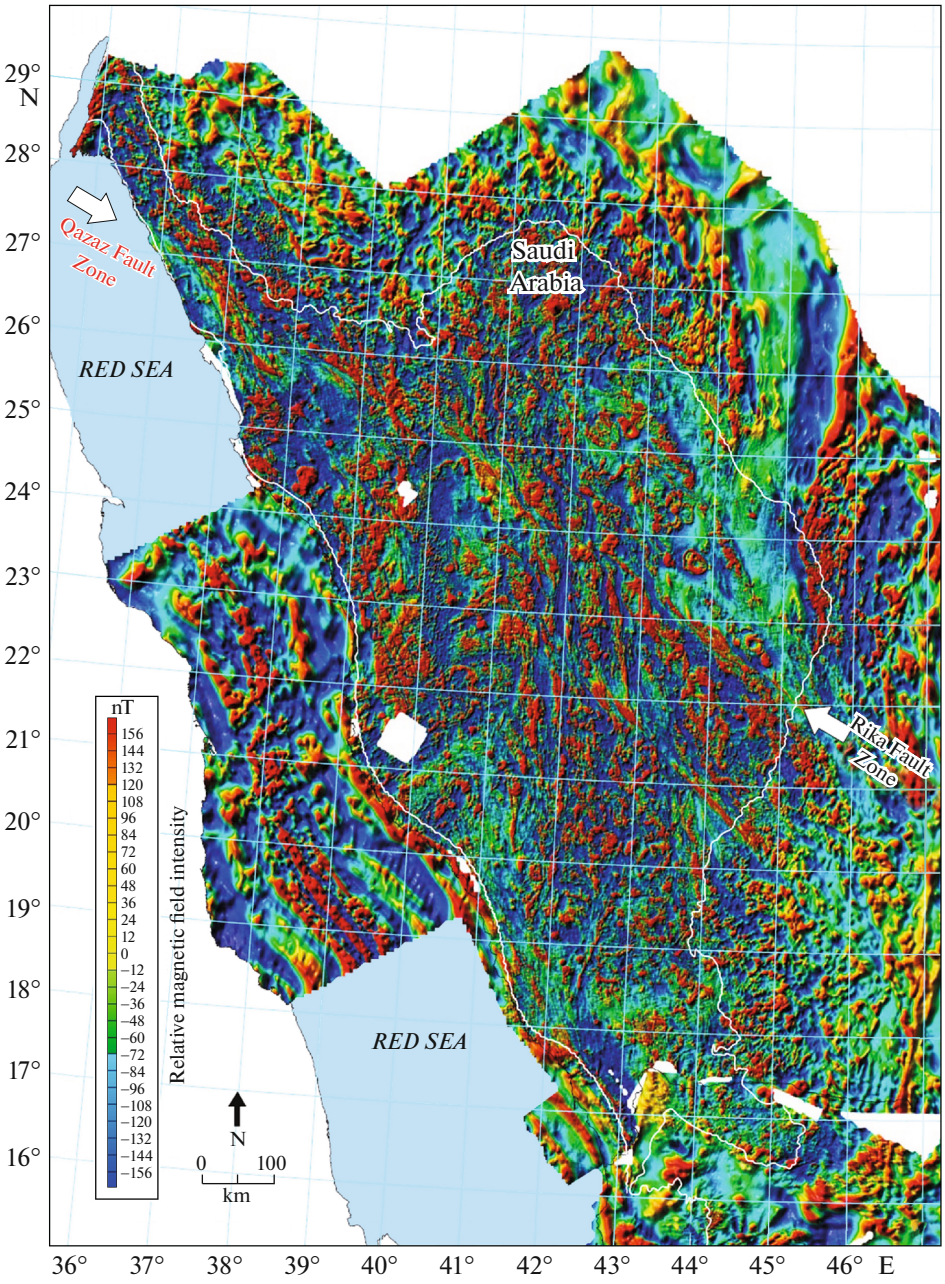

Fig. 12. Map of magnetic anomalies of the Arabian Shield recalculated to pole (after [124], modified). White spots in the map show areas not covered by magnetic survey on land.

causes the appearance of both clockwise and counterclockwise rotation. Outside the projection of the deep structure, the clockwise rotation prevails.

Transformed toward the pole, i.e., free from the influence of oblique magnetization, the map of magnetic anomalies of the Arabian Peninsula (Fig. 12) contains three heterogeneous zones differing in structure and belonging to the magnetization scale: (i) a linearly elongated zone of the Late Cenozoic stripe anomalies in the Red Sea, (ii) a complex system of fragmented reticular magnetization within the Neoproterozoic shield of the Arabian Plate, and (iii) a peripheral arcuate belt of linear anomalies.

Within the shield, magmatic bodies of the Neoproterozoic island arc complex and a system of Late Cenozoic dikes and traps overprinting an older system are magnetically active. The peripheral eastern zone curves around the Precambrian shield in an arcuate manner; the trend of its linear anomalies coincides with the arcuate distribution of GPS vectors and is close to the trend of isolines of the deep mantle structure. This indicates the influence of a deep anomalous

object on rocks occurring at the depths of no more than several tens of kilometers.

The regional trend of satellite gravitational anomalies and gravitational anomalies in Cyprus (at the geometric center of the deep structure projection) and in the Red Sea rift zone (along the long axis of the projection of the deep mantle structure) perfectly agree with each other (Fig. 6). The map of thicknesses of the lithosphere derived from the satellite gravimetric data shows not only the geodynamic asymmetry of the eastern and western coasts of the Red Sea, but also some elements of counterclockwise rotation (Fig. 11). The nearly ideal coincidence of the critical latitude 35° [77, 120] and high-intensity Cyprus gravitational anomaly [46] with the center of the revealed mantle structure [37] cannot be random [74].

The obtained geophysical data confirm the Trubitsyn's theoretical calculations [113], which showed that a depth of 1650–1700 km corresponds to the anomalous zone of the spin (phase) transition, which coincides with the position of the upper edge of the discovered mantle structure. Such zones are the most unstable and often include mantle plumes, which can affect the geodynamics and magmatism of the upper mantle and crustal layers, as well as the characteristics of sedimentary basins occurring in near-surface layers [114].

Two axial positions of the deep structure projection marked by Mesozoic and Cenozoic trap complexes are a natural structural limitation of the Sinai Plate as an independent geodynamic structure [10] (Fig. 10).

Such wide development of Mesozoic and Cenozoic trap basins and intrusive manifestations forming linearly elongated structures in the study region requires theoretical substantiation. It is interesting to note that many authors [66, 102] argue that the conventional plate tectonics cannot explain or predict intraplate (platform) magmatism (traps, flood basalts, kimberlites) and the corresponding metallogeny. At the same time, the identified deep mantle structure may theoretically explain the origin of linear structures of the continental magmatism, which remains insufficiently substantiated in the tectonic–geophysical aspect [107]. The zones of development of Neogene effusive traps and dike complexes, as well as places of discovery of the Cretaceous diamonds in Egypt, Israel, and Syria, are consistent with the long axis of the revealed structure (Fig. 10).

The overall coincidence of the large body of paleotectonic data for this region of Gondwana (such as the large Heletz dome) (Fig. 2) with data obtained from deep geophysical analysis seems to be especially significant. For example, a vast regional uplift zone stretching submeridionally was mapped, the axis of which coincides with the Arabian boundary zone [53]. The arch of the structure, where even the uppermost layers of the Precambrian are absent—arkoses of the Zenifim Formation—have been determined from the Heletz terrane and partly from the autochthonous block of the Sinai Peninsula.

The eastern flank of this uplift contains younger formations of the Lower Paleozoic—from the Cambrian to the Silurian and beyond—to formations of the Upper Paleozoic. Without delving into the problems of the allochthonous nature of a number of structures attributed to this uplift, we note that the axis of this vast paleotectonic structure of Gondwana coincides with the early (Late Paleozoic–Mesozoic) position of the axis of the revealed deep mantle structure.

The constructed physical–geological model proves the existence of the giant mantle ring structure and is based on integration of the following geophysical–geological factors:

(1) calculation of the cubic polynomial trend of satellite gravimetric data indicating an circular (ellipsoidal) structure,

(2) the results of quantitative interpretation of the polynomial gravitational anomaly,

(3) calculation of residual gravitational anomalies for the lower mantle,

(4) circular position of the GPS vector distribution,

(5) anomalous pattern of the geoid,

(6) seismotomographic data,

(7) paleomagnetic data indicating predominant counterclockwise rotation of crustal blocks,

(8) numerous mineralogical and petrological data indicating tectonic and geodynamic activity within the projection of the deep mantle structure onto the near-surface part of the geological section,

(9) geodynamic conclusions about conjugate deformation of the Earth's ellipsoid along latitude 35°, where the center of the revealed structure is located,

(10) paleobiogeographic data,

(11) numerous tectonic–structural data.

It is highly unlikely that these independent significant factors accidentally coincide (given that we consider only the main indicators) [74].

CONCLUSIONS

This detailed study sheds light on the relationship between a previously unknown deep mantle structure and subsurface geological and geophysical features of the geological setting. The authors comprehensively studied this relationship, taking into account the various interrelated components of this deep structure.

(1) The presence of a deep rotating ring structure is reflected in a wide range of independent data obtained by various research methods: polynomially processed satellite gravimetric data (i), quantitative analysis of polynomial gravitational anomalies (ii), calculation of residual gravitational anomalies for the lower mantle (iii), seismic tomography (iv), distribution of GPS monitoring vectors (v), analysis of paleomag-

netic data (vi), analysis of geoid anomalies (vii), analysis of geodynamic data (viii), analysis of tectonic indicators (ix), paleobiogeographic reconstructions, as well as numerous confirmations obtained from analyzing tectonic–structural, geodynamic, petrological, and mineralogical data (x). The probabilistic estimate of a random coincidence of all these factors is extremely small.

(2) The discovery of a deep anomalous structure explains, in particular, the existence of intraplatform magmatic belts that had not previously found logical explanation within the framework of existing theories.

(3) The discovered deep ring structure, influencing many tectonic–geodynamic processes, may be a global geodynamic factor contributing to spreading of the Red Sea. For the first time, the regional asymmetry of the Red Sea Basin has been revealed and interpreted in terms of tectonics and magmatism. We believe that this structure affects the Cyprus high-amplitude gravitational anomaly, the configuration of the Sinai Plate, counterclockwise rotation of the Mesozoic terrane belt, geometry of asymmetric basins along the Dead Sea Transform, and movement of the tectonic block corresponding to the Kiama paleomagnetic hyperzone in the Eastern Mediterranean.

ACKNOWLEDGMENTS

The authors express their heartfelt gratitude to *Geotectonics* editor M.N. Shoupletsova (Geological Institute, Russian Academy of Sciences, Moscow) for thoughtful and highly professional editing of the article; to Prof. E.A. Rogozhin (Schmidt Institute of Physics of the Earth, Russian Academy of Sciences, Moscow); and to the anonymous referee, whose remarks and comments helped significantly improve the article.

REFERENCES

1. J. H. Ahlberg, E. N. Nilson, and J. N. Walsh, *The Theory of Splines and Their Applications* (Academic, New York, 1967).
2. A. L. Aleinikov, V. T. Belikov, and L. V. Eppel'baum, *Some Physical Fundamentals of Geodynamics* (Kedem, Tel Aviv, 2001) [in Russian].
3. A. A. Alizadeh, I. S. Guliyev, F. A. Kadirov, and L. V. Eppelbaum, *Geosciences of Azerbaijan*, Vol. 1: *Geology* (Springer, Heidelberg, 2016).
4. D. L. Andersson, *New Theory of the Earth*, 2nd ed. (Cambridge Univ. Press, Cambridge, 2007).
5. I. Artemieva, H. Thybo, and M. K. Kaban, "Deep Europe today: Geophysical synthesis of the upper mantle structure and lithospheric processes over 3.5 Ga," in *European Lithosphere Dynamics*, Vol. 32 of *Geol. Soc. London., Mem.*, Ed. by D. G. Gee and R. A. Stephenson (London, 2006), pp. 11–41.
6. A. A. S. Barakat and M. R. Kandil, "Diamond in the newly discovered kimberlite and related rocks, Central Eastern Desert, Egypt," *Proceedings of the XXXVI International Conference "Magmatism of the Earth and Related Strategic Metal Deposits," St. Petersburg, Russia, 2019* (St. Petersburg Univ., St. Petersburg 2019), pp. 36–42.
7. E. J. Barbeau, *Polynomials* (Springer, New York, 2003).
8. H. J. Bayer, H. Hotzl, A. R. Jado, B. Ruscher, and W. Voggenreiter, "Sedimentary and structural evolution of the northwest Arabian Red Sea margin," Tectonophysics **153**, 137–151 (1988).
9. M. L. Bazhenov, and V. S. Burtman, "Eocene paleomagnetism of the Caucasus (southwest Georgia): Oroclinal bending in the Arabian syntaxis," Tectonophysics **344**, 247–259 (2002).
10. Z. Ben-Avraham, "The structure and tectonic setting of the Levant continental margin, Eastern Mediterranean," Tectonophysics **46**, 313–331 (1978).
11. Z. Ben-Avraham, "Structural framework of the Gulf of Elat (Aqaba), northern Red Sea," J. Geophys. Res., [Solid Earth Planets] **90**, 703–726 (1985).
12. Z. Ben-Avraham, "Development of asymmetric basins along continental transform faults," Tectonophysics **215**, 209–220 (1992).
13. Z. Ben-Avraham and A. Ginzburg, "Displaced terranes and crustal evolution of the Levant and the Eastern Mediterranean," Tectonics **9**, 613–622 (1990).
14. Z. Ben-Avraham, A. Ginzburg, J. Makris, and L. Eppelbaum, "Crustal structure of the Levant basin, eastern Mediterranean," Tectonophysics **346**, 23–43 (2002).
15. Z. Ben-Avraham, U. ten-Brink, R. Bell, and M. Reznikov, "Gravity field over the Sea of Galilee: Evidence for a composite basin along a transform fault," J. Geophys. Res.: Solid Earth **101**, 533–544 (1996).
16. G. J. Borradaile, F. Lagroix, T. D. Hamilton, and D. A. Trebilcock, "Ophiolite tectonics, rock magnetism and paleomagnetism, Cyprus," Surv. Geophys. **31**, 285–359 (2010).
17. G. J. Borradaile, and K. Lucas, "Tectonics of the Akamas and Mamonia ophiolites, Western Cyprus: Magnetic petrofabrics and paleomagnetism," J. Struct. Geol. **25**, 2053–2076 (2003).
18. L. Boschi, C. Faccenna, and T. W. Becker, "Mantle structure and dynamic topography in the Mediterranean basin," Geophys. Res. Lett. **37**, Art. No. L20303 (2010). https://doi.org/10.1029/2010GL045001
19. W. Bosworth, P. Huchon, and K. McClay, "The Red Sea and Gulf of Aden Basins," J. Afr. Earth Sci. **43**, 334–378 (2005).
20. V. Yu. Burmin and L. A. Shumlyanskaya, "The modern seismicity of the Crimea," Vopr. Inzh. Seismol. **42** (2), 5–17 (2009).
21. G. H.-N. Chan, J. Malpas, C. Xenophontos, and C.-H. Lo, "Magmatism associated with Gondwanian rifting and Neo-Tethyan oceanic basin development: Evidence from the Mamonia Complex, SW Cyprus," J. Geol. Soc. (London, U. K.) **165**, 699–709 (2008).
22. S. Cloetingh and S.D. Willet, "Linking deep Earth and surface processes," EOS, Trans. Am. Geophys. Union **94**, 53–54 (2013).

23. S. Cloetingh, A. Tibaldi, L. Dobrzhinetskaya, L. Matenco, F. Nader, and B. v. W. de Vries, "From the deep Earth to the surface: A multiscale approach," Global Planet. Change **171**, 1–322 (2018).

24. V. Cvetković, K. Šarić, D. Prelević, J. Genser, F. Neubauer, V. Höck, and A. Von Quadt, "An anorogenic pulse in a typical orogenic setting: The geochemical and geochronological record in the East Serbian latest Cretaceous to Palaeocene alkaline rocks," Lithos **180–181**, 181–199 (2013).

25. Y. Çubuk-Sabuncu, T. Taymaz, and A. Fichtner, "3-D crustal velocity structure of western Turkey: Constraints from full-waveform tomography," Phys. Earth Planet. Inter. **270**, 90–112 (2017).

26. L. Dobrzhinetskaya, P. Mukhin, Q. Wang, R. Wirth, E. O'Bannon, W. Zhao, L. Eppelbaum, and T. Sokhonchuk, "Moissanite (SiC) with metal-silicide and silicon inclusions from tuff of Israel: Search for a primary source," Lithos **310–311**, 355–368 (2018).

27. C. Doubre, A. Déprez, F. Masson, A. Socquet, E. Lewi, R. Grandin, A. Nercessian, P. Ulrich, J.-B. De Chabalier, I. Saad, A. Abayazid, G. Peltzer, A. Delorme, E. Calasis, and T. Wright, "Current deformation in Central Afar and triple junction kinematics deduced from GPS and InSAR measurements," Geophys. J. Int. **208,** 936–953 (2017).

28. C. E. Duermeijer, W. Krijgsman, C. G. Langereis, and J. H. Ten Veen, "Post-early Messinian counterclockwise rotations on Crete: Implications for Late Miocene to Recent kinematics of the southern Hellenic arc," Tectonophysics **298**, 177–189 (1998).

29. M. N. Elgabry, G. F. Panza, A. A. Badawy, and M. K. Ibrahim, "Imaging a relic of complex tectonics: the lithosphere asthenosphere structure in the Eastern Mediterranean," Terra Nova **25**, 102–109 (2013).

30. S. A. El-Quliti, T. B. S. Al-Harbi, M. B. S. Al-Yami, A. B. M. Al-Ghamdi, and M. B. M. Al-Shammari, "Assessment of Main Parameters of Extreme earthquakes in Red Sea, West Coast of Saudi Arabia," Open J. Earthquake Res. **5**, 122–134 (2016).

31. L. V. Eppelbaum, Z. Ben-Avraham, and Y. I. Katz, "Structure of the Sea of Galilee and Kinarot Valley derived from combined geological-geophysical analysis," First Break **25**, 21–28 (2007).

32. L. V. Eppelbaum, A. V. Nikolaev, and Yu. I. Kats, "Spatial position of the Kiama inverse magnetization zone in the oceanic crust of the Eastern Mediterranean," Dokl. Earth Sci. **457**, 1034–1038 (2014).

33. L. V. Eppelbaum, and Y. I. Katz, "Key features of seismo-neotectonic pattern of the Eastern Mediterranean," Izv., Acad. Sci. Azerb. Rep., Ser.: Earth Sci., No. 3, 29–40 (2012).

34. L. V. Eppelbaum, and Yu. I. Katz, "Eastern Mediterranean: Combined geological-geophysical zonation and paleogeodynamics of the Mesozoic and Cenozoic structural-sedimentation stages," Mar. Pet. Geol. **65**, 198–216 (2015).

35. L. V. Eppelbaum and Yu. I. Katz, "Newly developed paleomagnetic map of the easternmost Mediterranean unmasks geodynamic history of this region," Central Eur. J. Geosci. **7** (1), 95–117 (2015).

36. L. V. Eppelbaum and Yu. I. Katz, "A new regard on the tectonic map of the Arabian-African region inferred from the satellite gravity analysis," Acta Geophys. **65**, 607–626 (2017).

37. L. Eppelbaum and Yu. Katz, "Significant tectono-geophysical features of the African-Arabian tectonic region: An overview," Geotectonics **54**, 266–283 (2020).

38. L. Eppelbaum, Yu. Katz, J. Klokochnik, J. Kosteletsky, Z. Ben-Avraham, and V. Zheludev, "Tectonic insights into the Arabian-African region inferred from a comprehensive examination of satellite gravity big data," Global Planet. Change **171**, 65–87 (2018).

39. L. V. Eppelbaum and B. E. Khesin, *Geophysical Studies in the Caucasus* (Springer, Heidelberg, 2012).

40. L. V. Eppelbaum, V. L. Vaksman, S. V. Kuznetsov, L. V. Sazonova, S. A. Smirnov, A. V. Surkov, B. M. Bezlepkin, Yu. I. Kats, N. N. Korotaeva, and G. I. Belovitskaya, "Discovery of microdiamonds and associated minerals in the Makhtesh Ramon Canyon (Negev Desert, Israel)," Dokl. Earth Sci. **407**, 202–204 (2006).

41. S. Esperanza and Z. Garfunkel, "Ultramafic xenoliths from the Mt Carmel area (Karem Maharal Volcano), Israel," Lithos **19**, 43–49 (1986).

42. C. Faccenna, T. W. Becker, L. Auer, A. Billi, L. Boschi, J. P. Brun, F.A. Capitanio, F. Funiciello, F. Horvàth, L. Jolivet, C. Piromallo, L. Royden, F. Rossetti, and E. Serpelloni, "Mantle dynamics in the Mediterranean," Rev. Geophys. **52**, 283–332 (2014).

43. C. Faccenna, L. Jolivet, C. Piromallo, and A. Morelli, "Subduction and depth of convection in the Mediterranean mantle," J. Geophys. Res.: Solid Earth **108** (2003).
https://doi.org/10.1029/2001JB001690

44. Z. Garfunkel and Z. Ben-Avraham, "The structure of the Dead Sea basin," Tectonophysics 266, 155–176 (1996).

45. M. S. Garson and M. Krs, "Geophysical and geological evidence of the relationship of Red Sea transverse tectonics to ancient fractures," Geol. Soc. Am. Bull. **87**, 169–181 (1976).

46. I. G. Gass, "Is the Troodos Massif of Cyprus a fragment of Mesozoic ocean floor?," Nature **220** (5162), 39–42 (1968).

47. I. G. Gass, and D. Masson-Smith, "The geology and gravity anomalies of the Troodos Massif, Cyprus," Philos. Trans. R. Soc. London, Ser. A **255**, 417–466 (1963).

48. R. P. George, Jr., "Structural petrology of the Olympus ultramafic complex in the Troodos ophiolite, Cyprus," Geol. Soc. Am. Bull. **89**, 845–865 (1978).

49. S. Godey, R. Bossu, J. Guilbert, and G. Mazet-Roux, "The Euro-Mediterranean Bulletin: A comprehensive seismological bulletin at regional scale," Seismol. Res. Lett. **77**, 460–474 (2006).

50. W. L. Griffin, S. E. M. Gain, D.T. Adams, J.-X. Huang, M. Saunders, V. Toledo, N. J. Pearson, and S. Y. O'Reilly, "First terrestrial occurrence of tistarite (Ti_2O_3): Ultra-low oxygen fugacity in the upper mantle beneath Mount Carmel, Israel," Geology **44**, 815–818 (2016).

51. A. A. Khalafly, *Paleomagnetism of the Lesser Caucasus* (Takhsil, Baku, 2006) [in Russian].

52. A. A. Khalafov, "Magnetic studies of Coniacian–Santonian deposits from the Gazakh Depression," Izv. Akad. Nauk Azerb. SSR. Ser. Nauki Zemle, No. 4, 123–126 (1986).

53. J. K. Hall, V. A. Krasheninnikov, F. Hirsch, C. Benjamini, and A. Flexer, *Geological Framework of the Levant*, Vol. 2: *The Levantine Basin and Israel* (Historical Productions-Hall, Jerusalem, Israel, 2005).

54. M. Hässig, Y. Rolland, and M. Sosson, "From seafloor spreading to obduction: Jurassic–Cretaceous evolution of the northern branch of the Neotethys in the Northeastern Anatolian and Lesser Caucasus regions," in *Tectonic Evolution of the Eastern Black Sea and Caucasus*, Vol. 428 of *Geol. Soc. London, Spec. Publ.*, Ed. by M. Sosson, R. A. Stephenson, and S. A. Adamia (London, 2010), pp. 1–20.

55. B. Henry, C. Homberg, M. Mroueh, W. Hamdan, and W. Higazi, "Rotations in Lebanon inferred from new palaeomagnetic data and implications for the evolution of the Dead Sea Transform system," in *Evolution of the Levant Margin and Western Arabia Platform since the Mesozoic*, Vol. 341 of *Geol. Soc. London, Spec. Publ.*, Ed. by C. Homberg and M. Bachman (London, 2010), pp. 269–285.

56. Z. Z. M. Hisarli, "New paleomagnetic constraints on the Late Cretaceous and Early Cenozoic tectonic history of the Eastern Pontides," J. Geodyn. **52**, 114–128 (2011).

57. E. H. Ibrahim, H. H. Odah, H. L. El Agami, and M. Abu El Enen, "Paleomagnetic and geological investigation into southern Sinai volcanic rocks and the rifting of the Gulf of Suez," Tectonophysics **321**, 343–358 (2000).

58. T. A. Ismail-zade, Doctoral Dissertation in Geology and Mineralogy (Moscow, 1983).

59. L. Jolivet, C. Faccenna, P. Agard, D. F. de Lamotte, A. Menant, P. Sternai, and F. Guillocheau, "Neo-Tethys geodynamics and mantle convection: From extension to compression in Africa and a conceptual model for obduction," Can. J. Earth Sci. **53**, 1–15 (2016).

60. M. K. Kaban, S. El Khrepy, N. Al-Arifi, M. Tesauro, and W. Stolk, "Three dimensional density model of the upper mantle in the Middle East: Interaction of diverse tectonic processes," J. Geophys. Res., Ser.: Solid Earth **121**, 5349–5364 (2016).

61. M. K. Kaban, S. El Khrepy, and N. Al-Arifi, "Importance of the decompensative correction of the gravity field for study of the upper crust: Application to the Arabian plate and surroundings," Pure Appl. Geophys. **174**, 349–358 (2017).

62. M. K. Kaban, A. G. Petrunin, S. El Khrepy, and N. Al-Arifi, "Diverse continental subduction scenarios along the Arabia–Eurasia collision zone," Geophys. Res. Lett. **45**, 6898–6906 (2018).

63. Yu. I. Kats, "New kinds of the Late Cretaceous castle brachiopods from the Tajik Depression and adjacent regions," Uch. Zap. Khar'k. Gos. Univ., Otd. Geol. **15**, 132–154 (1962).

64. Yu. I. Kats, "Cretaceous thalassocratic maximum and planetary movements of the hydrosphere," in *The Cretaceous Period: Paleogeography and Paleooceanology*, Ed. by N. P. Vasil'kovskii (Nauka, Moscow, 1986), pp. 191–237.

65. V. G. Kaz'min, *Rift Structures of East Africa: Continental Breakup and Nucleation of the Ocean* (Nauka, Moscow, 1987) [in Russian].

66. V. E. Khain, *Tectonics of Continents and Oceans* (Nauchnyi Mir, Moscow, 2001) [in Russian].

67. V. E. Khain and N. V. Koronovskii, *Planet Earth: From the Core to The Ionosphere* (Mosk. Gos. Univ., Moscow, 2007) [in Russian].

68. B. E. Khesin, V. V. Alexeyev, and L. V. Eppelbaum, *Interpretation of Geophysical Fields in Complicated Environments*, Vol. 14 of *Mod. Approaches Geophys.* (Kluwer, Dordrecht, 1996).

69. A. N. Khramov, *Paleomagnetic Directions and Pole Positions: Data for the USSR (Catalogue)*, No. 1 of *World Data Center, Ser. B* (Geofiz. Kom. Akad. Nauk SSSR, Moscow, 1984).

70. A. N. Khramov, *Paleomagnetology* (Springer, Berlin, 1987).

71. C. Kissel, C. Laj, A. Poisson, and N. Görür, "Paleomagnetic reconstruction of the Cenozoic evolution of the Eastern Mediterranean," Tectonophysics **362**, 199–217 (2003).

72. D. Kondopoulou, I. Zananiri, A. Michard, H. Feinberg, A. Atzemoglou, J.-P. Pozzi, and Ph. Voidomatis, "Neogene tectonic rotations in the vicinity of the north Aegean trough: New paleomagnetic evidence from Athos and Samothraki (Greece)," Bull. Geol. Soc. Greece **40**, 343–359 (2007).

73. M. L. Kopp, *Mobilistic Theory of the Platforms in Northeastern Europe* (Nauka, Moscow, 2004) [in Russian].

74. L. Koralov and Y. G. Sinai, *Theory of Probability and Random Processes*, 2nd ed. (Springer, Berlin, 2007).

75. C. Krézsek, A. Lăpădat, L. Maţenco, K. Arnberger, V. Barbu, and R. Olaru, "Strain partitioning at orogenic contacts during rotation, strike–slip and oblique convergence: Paleogene–Early Miocene evolution of the contact between the South Carpathians and Moesia Csaba," Global Planet. Change **103**, 63–81 (2013).

76. F. G. Lemoine, et al., "The NASA and DMA joint geopotential model," EOS, Trans. Am. Geophys. Union **77** (Fall Meet. Suppl.), Abstr. No. F136 (1996).

77. B. V. Levin, E. V. Sazorova, and A. V. Domanskii, "Properties of critical latitudes in variations of rotation with respect to seismicity of the Earth," Vestn. Dal'nevost. Otd. Ros. Akad. Nauk, No. 3, 3–8 (2013).

78. H. I. Lotfi, "Early Cretaceous counterclockwise rotation of Northeast Africa within the equatorial zone: Paleomagnetic study on Mansouri ring complex, Southeastern Desert, Egypt," NRIAG J. Astron. Geophys. **4** (1), 1–15 (2015).

79. J. Makris, C. H. Henke, F. Egloff, and T. Akamaluk, "The gravity field of the Red Sea and East Africa," Tectonophysics **198**, 369–381 (1991).

80. J. Makris and R. Rihm, "Shear-controlled evolution of the Red Sea: Pull-apart model," Tectonophysics **198**, 441–466 (1991).

81. P. Marchev, R. Raicheva, H. Downes, O. Vaselli, M. Chiaradia, and R. Moritz, "Compositional diversity of Eocene–Oligocene basaltic magmatism in the Eastern Rhodopes, SE Bulgaria: Implications for genesis and tectonic setting," Tectonophysics **393**, 301–328 (2004).
82. E. Márton, J. Grabowski, D. Plašienka, I. Túnyi, M. Krobicki, J. Haas, and M. Pethe, "New paleomagnetic results from the Upper Cretaceous red marls of the Pieniny Klippen Belt, Western Carpathians: Evidence for general CCW rotation and implications for the origin of the structural arc formation," Tectonophysics **592**, 1–13 (2013).
83. S. McClusky, S. Balassanian, A. Barka, C. Demir, S. Ergintav, I. Georgiev, O. Gürkan, M. Hamburger, K. Hurst, H. Kahle, K. Kastens, G. Kekelidze, R. King, V. Kotzev, O. Lenk, et al., "Global Positioning System constraints on plate kinematics and dynamics in the eastern Mediterranean and Caucasus," J. Geophys. Res.: Solid Earth **105**, 5695–5719 (2000).
84. A. Menant, L. Jolivet, and B. Vrielynck, "Kinematic reconstructions and magmatic evolution illuminating crustal and mantle dynamics of the eastern Mediterranean region since the late Cretaceous," Tectonophysics **675**, 103–140 (2016).
85. A. Morris, M. W. Erson, A. H. Robertson, and K. Al-Riyami, "Extreme tectonic rotations within an eastern Mediterranean ophiolite (Baër–Bassit, Syria)," Earth Planet. Sci. Lett. **202**, 247–261 (2002).
86. A. A. Muluneh, M. Cuffaro, and C. Doglioni, "Left-lateral transtension along the Ethiopian Rift and constrains on the mantle-reference plate motions," Tectonophysics **632**, 21–31 (2014).
87. G. Muttoni, E. Erba, D. V. Kent, and V. Bachtadse, "Mesozoic Alpine facies deposition as a result of past latitudinal plate motion," Nature **434**, 59–63 (2005).
88. G. Muttoni, D. V. Kent, E. Garzanti, P. Brack, N. Abrahamsen, and M. Gaetani, "Early Permian Pangea 'B' to Late Permian Pangea 'A'," Earth Planet. Sci. Lett. **215**, 379–394 (2003).
89. A. I. Okay and A. Tuysuz, "Tethyan sutures of northern Turkey," in *The Mediterranean Basins: Tertiary Extension within the Alpine Orogen*, Vol. 156 of *Geol. Soc., London, Spec. Publ.*, Ed. by B. Durand, L. Jolivet, F. Horvath, and M. Seranne (London, 1999), pp. 475–515.
90. D. M. Pecherskii and T. K. Nguen, *Paleomagnetic Directions and Pole Positions: Data for the USSR (Catalogue)*, No. 4 of *World Data Center, Ser. B* (Geofiz. Kom. Akad. Nauk SSSR, Moscow, 1979).
91. R. E. Reilinger, S. McClusky, P. Vernant, S. Lawrence, S. Ergintav, R. Cakmak, H. Ozener, F. Kadirov, I. Guliev, R. Stepanyan, M. Nadariya, G. Hahubia, S. Mahmoud, K. Sakr, A. ArRajehi, et al., "GPS constraints on continental deformation in the Africa–Arabia–Eurasia continental collision zone and implications for the dynamics of plate interactions," J. Geophys. Res.: Solid Earth **111**, Art. No. BO5411 (2006). https://doi.org/10.1029/2005JB004051
92. H. V. Renngarten and Z. M. Starostina, "Geological and lithologic studies of Lias sediments on the northern slope of central Caucasus," in *Geology and Mineral Resources of the Central Part of Northern Caucasus*, Ed. by E. V. Brizke (Akad. Nauk SSSR, Moscow, 1956), pp. 83–147.
93. M. A. Richards and B. H. Hager, "Geoid anomalies in a dynamic Earth," J. Geophys. Res., B **89**, 5987–6002 (1984).
94. Y. Rolland, "Caucasus collisional history: Review of data from East Anatolia to West Iran," Gondwana Res. **49**, 130–146 (2017).
95. Y. Rolland, M. Hässig, D. Bosch, D. Bruguier, R. Melis, G. Galoyan, G. Topuz, L. Sahakyan, A. Avagyan, and M. Sosson, "The East Anatolia–Lesser Caucasus ophiolite: An exceptional case of large-scale obduction, synthesis of data and numerical modelling," Geosci. Front. **11**, 83–108 (2020).
96. H. Ron, R. Freund, Z. Garfunkel, and A. Nur, "Block rotation by strike-slip faulting: structural and paleomagnetic evidence," J. Geophys. Res., B **89**, 6256–6270 (1984).
97. D. T. Sandwell, E. Garcia, K. Soofi, P. Wessel, M. Chandler, and W. H. F. Smith, "Toward 1-mGal global marine gravity from CryoSat-2, Envisat, and Jason-1," The Leading Edge **32**, 892–899 (2013).
98. A. J. Schaeffer and S. Lebedev, "Global shear-speed structure of the upper mantle and transition zone," Geophys. J. Int. **194**, 417–449 (2013).
99. C. Schmid, S. van der Lee, J. C. VanDecar, E. R. Engdahl, D. Giardini, "Three-dimensional S velocity of the mantle in the Africa-Eurasia plate boundary region from phase arrival times and regional waveforms," J. Geophys. Res.: Solid Earth **113**, Art. No. B03306 (2008). https://doi.org/10.1029/2005JB004193
100. E. V. Sharkov and S. Khanna, "Evolution of the upper mantle material in regions of intraplate magmatism: Case study of western Syria," Dokl. Akad. Nauk SSSR **297**, 684–686 (1987).
101. N. S. Shatskii, A. A. Belyaevskii, A. N. Bogdanov, and M. E. Muratov, *Tectonic Map of the USSR and Adjacent Countries, Scale 1 : 5000000* (Gosgeoltekhizdat, Moscow, 1956).
102. E. A. Skobelin, I. P. Sharapov, and A. F. Bugayov, "Deliberations of state and ways of perestroika in geology (Has plate tectonics resulted in a revolution in geology?)," in *Critical Aspects of the Plate Tectonics Theory* (Theophrastus Publ., Athens, Greece, 1990), Vol. 1, pp. 17–37.
103. J. Smit, J.-P. Brun, S. Cloetingh, and Z. Ben-Avraham, "The rift-like structure and asymmetry of the Dead Sea Fault," Earth Planet. Sci. Lett. 290, 74–82 (2010).
104. A. Sneh, Y. Bartov, and M. Rozensaft, *Geological Map of Israel, Scale 1 : 200000* (Minist. Natl. Infrastruct., Jerusalem, 1998).
105. V. B. Sollogub, *Litosphere of Ukraine* (Naukova Dumka, Kiev, 1986) [in Russian].
106. G. M. Stampfli, C. Hochard, C. Vérard, C. Wilhem, and J. von Raumer, "The formation of Pangea," Tectonophysics **593**, 1–19 (2013).
107. B. Steinberger and A. R. Calderwood, "Models of large-scale viscous flow in the Earth's mantle with constraints from mineral physics and surface observations," Geophys. J. Int. **167**, 1461–1481 (2006).

108. R. J. Stern and P. R. Johnson, "Continental lithosphere of the Arabian Plate: A geologic, petrologic, and geophysical synthesis," Earth-Sci. Rev. **101**, 29–67 (2010).

109. W.-J. Su, R. L. Woodward, and A. M. Dziewonski, "Degree-12 model of shear velocity heterogeneity in the mantle," J. Geophys. Res.: Solid Earth **99**, 4945–4980 (1994).

110. R. N. Taylor and R.W. Nesbitt, "Light rare-earth enrichment of supra subduction-zone mantle: Evidence from the Troodos ophiolite, Cyprus," Geology **16**, P. 448–451 (1988).

111. W. M. Telford, L. R. Geldart, and R. E. Sheriff, *Applied Geophysics* (Cambridge Univ. Press, Cambridge, 1991).

112. M. Tesauro, M. K. Kaban, W. D. Mooney, and S. A. P. L. Cloetingh, "Density, temperature, and composition of the North American lithosphere—new insights from joint analysis of seismic, gravity, and mineral physics data: 2. Thermal and compositional model of the upper mantle," Geochem. Geophys. Geosyst. **15**, 4808–4830 (2014).

113. V. P. Trubitsyn, "The nature of the boundary between the upper and the lower mantle and its influence on convection," Izv., Phys. Solid Earth **46**, 461–476 (2010).

114. V. P. Trubitsyn, "Propagation of oceanic plates through the boundary between the upper and lower mantle," Dokl. Earth Sci. **446**, 1220–1222 (2012).

115. B. Uzel, C. G. Langereis, N. Kaymakci, H. Sözbilir, C. Özkaymak, and M. Özkaptan, "Paleomagnetic evidence for an inverse rotation history of Western Anatolia during the exhumation of Menderes core complex," Earth Planet. Sci. Lett. **414**, 108–125 (2015).

116. J. R. Vail, "Ring complexes and related rocks in Africa," J. Afr. Earth Sci. **8**, 19–40 (1989).

117. R. D. Van der Hilst, S. Widiyantoro, and E. R. Engdahl, "Evidence for deep mantle circulation from global tomography," Nature **386**, 578–584 (1997).

118. D. G. van der Meer, D. J. J. van Hinsbergen, and W. Spakman, "Atlas of the underworld: Slab remnants in the mantle, their sinking history, and a new outlook on lower mantle viscosity," Tectonophysics **723**, 309–448 (2018).

119. G. Vannucci, S. Pondrelli, S. Argnani, A. Morelli, P. Gasperini, and E. Boschi, "An Atlas of Mediterranean seismicity," Ann. Geophys. **47** (Suppl. No. 1), 247–306 (2004).

120. A. Véronnet, "Rotation de l'ellipsoide hétérogène et figure exacte de la terre," J. Math. Pures Appl., Ser. 6 **8**, 331–463 (1912).

121. L. Wen and D. V. Helmberger, "Ultra-low velocity zones near the core-mantle boundary from broadband PKP precursors," Science. 279, 1701–1703 (1998).

122. M. Wilson, A. E. Shimron, J. M. Rosenbaum, and J. Preston, "Early Cretaceous magmatism of Mount Hermon, Northern Israel," Contrib. Mineral. Petrol. **139**, 54–67 (2000).

123. T. E. Yancey, M. A. Wilson, and A. C. S. Mione, "The Ramonalinids: a new family of mound-building bivalves of the Early Middle Triassic," Paleontology 52, 1349–1361 (2009).

124. H. M. Zahran, I. C. F. Stewart, P. R. Johnson, and M. H. Basahel, *Aeromagnetic Anomaly Maps of Central and Western Saudi Arabia, Scale 1 : 2000000*, No. SGS-OF-2002-8 of *Saudi Geol. Surv. Open-File Rep.* (Saudi Geol. Surv., Jeddah, 2003).

125. M. Zare, H. Amini, P. Yazdi, K. Sesetyan, M. B. Demircioglu, D. Kalafat, M. Erdik, D. Giardini, M. A. Khan, and N. Tsereteli, "Recent developments of the Middle East catalog," J. Seismol. **18**, 749–772 (2014).

126. National Geospatial-Intelligence Agency, EGM2008 - WGS 84 Version. https://earth-info.nga.mil/GandG/wgs84/gravitymod/egm2008/egm08_wgs84.html. Accessed April 22, 2020.